

# Relativistic Structural Characterization of Molybdenum and Tungsten Disulfide Materials

**Micheal Arockiaraj<sup>a</sup>, Sandi Klavžar<sup>b,c,d</sup>, S. Ruth Julie Kavitha<sup>a\*</sup>,  
Shaguфа Mushtaq<sup>e</sup>, Krishnan Balasubramanian<sup>f</sup>**

<sup>a</sup>Department of Mathematics, Loyola College, Chennai 600034, India

<sup>b</sup>Faculty of Mathematics and Physics, University of Ljubljana, Slovenia

<sup>c</sup>Faculty of Natural Sciences and Mathematics, University of Maribor, Slovenia

<sup>d</sup>Institute of Mathematics, Physics and Mechanics, Ljubljana, Slovenia

<sup>e</sup>Department of Mathematics, Loyola College, University of Madras, Chennai 600034, India

<sup>f</sup>School of Molecular Sciences, Arizona State University, Tempe AZ 85287-1604, USA

## Abstract

The advent of two-dimensional transition metal dichalcogenides has triggered an interest in exploring a new class of high performance materials with intriguing physico-chemical attributes. Molybdenum and tungsten disulfides have attracted significant attention due to surface excitons and trions, and large spin-orbit effects in these compounds. Moreover, WS<sub>2</sub> is especially intriguing due to large relativistic effects which results in bound excitons at the edge and biexciton formation in the bilayers. Hence we present a relativistic topological model for the characterization of these two types of metal disulfides. We have employed relativistically weighted graph-theoretical methods for obtaining structural descriptors of these compounds by taking the different shapes on the boundaries and employing the topological cut techniques.

**Keywords:** Relativistic topological indices; cut method; monolayers; distance-based descriptors.

## 1 Introduction

A new class of two-dimensional monolayer materials is receiving considerable interest in recent years [1, 2] ever since the advent of 2D graphene materials with novel properties. However, most of the available 2D materials in the pristine forms are intrinsically nonmagnetic and this thus limits their

---

\*Corresponding author : juliesuresh91@gmail.com

range of applications. Hence it is desirable to explore such novel 2D materials with a robust intrinsic ferromagnetic order for optimizing the device applications. Subsequently, the transition metal dichalcogenides (TMDs) [2–4] have been identified as notable candidates for their exclusive ferromagnetism, optical properties, surface excitonic features, and their ability to intercalate and exfoliate, have all contributed to a wide range of applications [5]. Consequently, these materials find applications in a number of areas such as spintronics, energy harvesting, DNA sequencing and personalized medicine as they possess a unique combination of atomic-scale thickness, spin-orbit coupling, direct bandgap and other favorable electronic and mechanical properties [6, 7]. Tungsten disulfide in its 2D form exhibits strongly bound excitons even at the edge, trion fine structures and interesting spin dynamics attributed to a large spin-orbit splitting of the tungsten atoms, all of which result in unusual optical properties of WS<sub>2</sub> [8–12].

Recent advances in sample preparation, optical detection, transfer and manipulation of 2D materials have also triggered a resurgence of scientific and engineering interest in TMDs [3, 6, 14]. In particular, the monolayers of two-dimensional crystals are emphasized more in industrial aspects than their bulk structure as the reduced dimensions significantly enhance many physical characteristics [3, 6, 7, 14]. For instance, the indirect bandgap of 1.3 eV in the bulk phase of MoS<sub>2</sub> changes to a direct bandgap of 1.8 eV in single-layer form [15] thus opening the possibility of a wide range of optoelectronic applications [4, 16]. As there exists many such interesting layer-dependent properties in 2D materials which differ significantly from the properties of the bulk materials, the investigation of various methods to scale the monolayers from their bulk phase has gained its momentum in the recent years [3, 6, 7, 14, 17].

The transition metal disulfides MS<sub>2</sub> (M = Mo, W) are popular among the TMDs that exhibit ideal magnetic and electrical characteristics for exploring the valley-based optoelectronic applications [18]. Their strong in-plane bonding and weak out-of-plane interactions enable the exfoliation of two-dimensional layers of single unit cell thickness although in the case of WS<sub>2</sub> exfoliation is more difficult [11] due to a stronger binding between the layers caused by relativistic effects [19–21] of tungsten. The attainment of a single layer with atomic thickness [3, 17] has enhanced their technological importance as the monolayers exhibit exceptional attributes including amplification of electrical signals with less power consumption, ultralow standby power dissipation and high mobility rates [6]. The direct bandgap, the electronic structure of their monolayers and the propensity to form WS<sub>2</sub> nanotubes emphasize their key roles in various fields such as the lithium ion batteries (LIB) [10, 22], flexible electronic devices [23], photovoltaics [24] and valleytronics [25]. Furthermore, their abundant availability helps in achieving cost-effective thermoelectric devices when compared to other conventional materials like bismuth telluride, offering a unique opportunity of realizing flexible generators for

the wearable technology [6]. Recently Manzeli et al. [26] summarized the various methods used to synthesize these TMDs and their intriguing properties with particular attention to their topological phases.

Graph theory provides powerful and efficient tools for the topological characterization of the underlying structural features through connectivity of the network. Any problem that involves a graph structure can be analyzed and solved using graph-theoretical tools which in turn enlarge the scope of utilization in numerous areas of science and engineering. In particular, chemical graph theory deals with the characterization of the underlying topology by providing elegant structural descriptors that have the efficacy to correlate with the observed properties. It is largely applied to attain the quantitative characterization of material structures, thereby enabling the study of quantitative structure activity (QSAR), property (QSPR) and toxicity (QSTR) relationships of the 2D molecular structures [27, 28, 62].

Topological indices are molecular parameters, which numerically quantify the underlying network connectivity [30]. They are invariant to the labeling of vertices, and thus form a reliable starting point in the quantitative study of molecules compared to other computationally intensive quantum chemical techniques. In the past decades, numerous papers were devoted to the study of such topological descriptors owing to its ability of predicting the pharmacochemical and physico-chemical attributes of a compound theoretically [29, 31–36, 44]. Moreover, such mathematical classifications including hypercubes can have far reaching applications in chemistry including explorations into quantum similarity measures of the periodic table of elements [37] and periodicity of aromatic compounds [38].

Although a graph theoretical model only depicts the underlying topology of the materials and not the chemical or quantum features, significant progress has been made over the years to address this problem [39–41]. Recently a relativistic topological model was proposed [41] by incorporating relativistic quantum chemical structural parameters through weights assigned to each vertex and edge of the 2D network. In the current study, we employ the relativistic structural descriptors to characterizing 2D transition metal disulfides through relativistically weighted graphs.

## 2 Mathematical Preliminaries

A simple connected graph  $G$  comprises of a vertex set  $V(G)$  and an edge set  $E(G)$ . For any two vertices  $u, v \in V(G)$ , the distance  $d_G(u, v)$  between them is defined as the number of edges on a shortest path connecting them. Similarly, we define the distance between a vertex  $u$  and an edge  $f = ab$  as  $d_G(u, f) = \min\{d_G(u, a), d_G(u, b)\}$  and the distance between two edges  $e = uv$  and  $f = ab$  as  $D_G(f, g) = \min\{d_G(e, a), d_G(e, b)\}$ . The degree  $d_G(u)$  of a vertex  $u$  is the number of edges incident

to the vertex  $u$  and the degree  $d_G(e)$  of an edge  $e$  is defined as the number of edges adjacent to  $e$ . In view of the degrees of end vertices of the edge, the weighted bond measures of  $e = uv$  with respect to sum and product are defined as  $w_e^+(e) = d_G(u) + d_G(v)$  and  $w_e^*(e) = d_G(u)d_G(v)$  respectively. The neighborhood  $N_G(v)$  of a vertex  $v$  is the set of all vertices adjacent to the vertex  $v$  and the closeness sets of an edge  $e = uv \in E(G)$  are defined as follows:

$$\begin{aligned} N_u(e|G) &= \{x \in V(G) : d_G(u, x) < d_G(v, x)\}, \\ M_u(e|G) &= \{f \in E(G) : d_G(u, f) < d_G(v, f)\}. \end{aligned}$$

The counts of the sets  $N_u(e|G)$  and  $M_u(e|G)$  are denoted as  $n_u(e|G)$  and  $m_u(e|G)$ , respectively, and  $t_u(e|G)$  denotes their sum. The values of  $n_v(e|G)$ ,  $m_v(e|G)$  and  $t_v(e|G)$  are analogous. For  $K \subseteq E(G)$ , the vertex set of a quotient graph  $G/K$  consists of the connected components of the graph  $G - K$ , and two components  $C$  and  $D$  being adjacent if there exists an edge  $cd \in K$  such that  $c \in C$  and  $d \in D$ . A subgraph  $H$  of a graph  $G$  is said to be convex if for any two vertices  $u, v \in H$ , any shortest path between them in  $G$  lies completely in  $H$ , whereas  $H$  is an isometric subgraph if for every pair of vertices, the distance between them in both  $G$  and  $H$  are equal. An isometric subgraph of a hypercube is called a partial cube, where the hypercube  $Q_n$  of dimension  $n$  is defined as the Cartesian product of  $n$  copies of the complete graph  $K_2$ .

A strength-weighted graph [33]  $G_{sw} = (G, SW_V, SW_E)$  is a graph  $G$  in which the vertex and edge set are assigned a pair of strength-weighted functions  $(SW_V, SW_E)$  defined as follows:

- (i)  $SW_V = (w_v, s_v)$ , where  $w_v, s_v : V(G_{sw}) \rightarrow \mathbb{R}_0^+$  are vertex-weight and strength functions,
- (ii)  $SW_E = (w_e, s_e)$ , where  $w_e, s_e : E(G_{sw}) \rightarrow \mathbb{R}_0^+$  are edge-weight and strength functions.

The structural terminologies such as distance, neighborhood and the closeness sets in  $G_{sw}$  remains the same as that of the simple graph  $G$ , whereas the degree and the cardinality of closeness sets in  $G_{sw}$  are defined in the following.

$$\begin{aligned} d_{G_{sw}}(u) &= \sum_{x \in N_{G_{sw}}(u)} s_e(ux), \\ n_u(e|G_{sw}) &= \sum_{x \in N_u(e|G_{sw})} w_v(x), \\ m_u(e|G_{sw}) &= \sum_{x \in N_u(e|G_{sw})} s_v(x) + \sum_{f \in M_u(e|G_{sw})} s_e(f). \end{aligned}$$

Topological indices are molecular descriptors that are enumerated based on the above defined structural parameters of the graphs. Wiener index [29] is the first originated index while determining the physical properties of certain type of alkanes known as paraffins.

Table 1: Topological indices of  $G_{sw}$  where  $e = uv$ 

| Variants      | Mathematical Expressions   |
|---------------|--|
| Wiener        | $W(G_{sw}) = \sum_{\{u,v\} \subseteq V(G_{sw})} w_v(u)w_v(v)d_{G_{sw}}(u,v)$ $W_e(G_{sw}) = \sum_{\{u,v\} \subseteq V(G_{sw})} s_v(u)s_v(v)d_{G_{sw}}(u,v) + \sum_{\{e,f\} \subseteq E(G_{sw})} s_e(e)s_e(f)$ $D_{G_{sw}}(e,f) + \sum_{u \in V(G_{sw})} \sum_{f \in E(G_{sw})} s_v(u)s_e(f)d_{G_{sw}}(u,f)$ $W_{ev}(G_{sw}) = \frac{1}{2} \left( \sum_{\{u,v\} \subseteq V(G_{sw})} \{w_v(u)s_v(v) + w_v(v)s_v(u)\} d_{G_{sw}}(u,v) \right. \\ \left. + \sum_{u \in V(G_{sw})} \sum_{f \in E(G_{sw})} w_v(u)s_e(f)d_{G_{sw}}(u,f) \right)$ |
| Szeged        | $Sz_v(G_{sw}) = \sum_{e \in E(G_{sw})} s_e(e)n_u(e G_{sw})n_v(e G_{sw})$ $Sz_e(G_{sw}) = \sum_{e \in E(G_{sw})} s_e(e)m_u(e G_{sw})m_v(e G_{sw})$ $Sz_{ev}(G_{sw}) = \frac{1}{2} \sum_{e \in E(G_{sw})} s_e(e) [n_u(e G_{sw})m_v(e G_{sw}) + n_v(e G_{sw})m_u(e G_{sw})]$ $Sz_t(G_{sw}) = Sz_v(G_{sw}) + Sz_e(G_{sw}) + 2Sz_{ev}(G_{sw})$  |
| Padmakar-Ivan | $PI(G_{sw}) = \sum_{e \in E(G_{sw})} s_e(e) [m_u(e G_{sw}) + m_v(e G_{sw})]$   |
| Mostar        | $Mo(G_{sw}) = \sum_{e \in E(G_{sw})} s_e(e) n_u(e G_{sw}) - n_v(e G_{sw}) $ $w^+ Mo(G_{sw}) = \sum_{e \in E(G_{sw})} w_e^+(e) n_u(e G_{sw}) - n_v(e G_{sw}) $ $w^* Mo(G_{sw}) = \sum_{e \in E(G_{sw})} w_e^*(e) n_u(e G_{sw}) - n_v(e G_{sw}) $  |
| Edge-Mostar   | $Mo_e(G_{sw}) = \sum_{e \in E(G_{sw})} s_e(e) m_u(e G_{sw}) - m_v(e G_{sw}) $ $w^+ Mo_e(G_{sw}) = \sum_{e \in E(G_{sw})} w_e^+(e) m_u(e G_{sw}) - m_v(e G_{sw}) $ $w^* Mo_e(G_{sw}) = \sum_{e \in E(G_{sw})} w_e^*(e) m_u(e G_{sw}) - m_v(e G_{sw}) $  |
| Total-Mostar  | $Mo_t(G_{sw}) = \sum_{e \in E(G_{sw})} s_e(e) t_u(e G_{sw}) - t_v(e G_{sw}) $ $w^+ Mo_t(G_{sw}) = \sum_{e \in E(G_{sw})} w_e^+(e) t_u(e G_{sw}) - t_v(e G_{sw}) $ $w^* Mo_t(G_{sw}) = \sum_{e \in E(G_{sw})} w_e^*(e) t_u(e G_{sw}) - t_v(e G_{sw}) $  |
| Schultz       | $S(G_{sw}) = \sum_{\{u,v\} \subseteq V(G_{sw})} [w_v(v)[d_{G_{sw}}(u) + 2s_v(u)] + w_v(u)[d_{G_{sw}}(v) + 2s_v(v)]]d_{G_{sw}}(u,v)$  |
| Gutman        | $Gut(G_{sw}) = \sum_{\{u,v\} \subseteq V(G_{sw})} [d_{G_{sw}}(u) + 2s_v(u)][d_{G_{sw}}(v) + 2s_v(v)]d_{G_{sw}}(u,v)$   |

The Schultz index is a degree and distance-based topological index with significant chemical applications and properties [42] and its revised version is called Gutman index [43]. Szeged index and its other variants are bond-based indices that are used to analyze the bond properties of the molecular compound [34, 35]. Mostar and its variants are recently synthesized descriptors for scrutinizing the peripheral property of the compound [31, 36]. The formulae of several topological indices ( $TI$ ) of a strength-weighted graph  $G_{sw}$  that are analyzed in this study are tabulated in Table 1, where  $TI(G_{sw}) = TI(G)$  if  $w_v = 1$ ,  $s_v = 0$ ,  $w_e = 1$  and  $s_e = 1$ .

The computational techniques for evaluating these indices continues to be an interesting topic of research [31–33, 44, 45] because it facilitates the topological characterization without actually calculating the numerical parameters of the graph. The cut method is a classical computational procedure [45] employed to investigate topological indices and is being revamped till date based on the kind of graphs [31, 33–35]. In this method, the key role is played by the Djoković–Winkler relation  $\Theta$  [46, 47]. This relation is defined on the edge set of a given graph  $G$ , where edges  $e = uv$  and  $f = ab$  of  $G$  are in relation  $\Theta$  if  $d_G(v, b) + d_G(u, a) \neq d_G(u, b) + d_G(v, a)$ .

The relation  $\Theta$  is reflexive and symmetric in general, but need not be transitive. In the bipartite case,  $\Theta$  is transitive precisely on partial cubes. In general, the transitive closure  $\Theta^*$  forms an equivalence relation, and thus partitions  $E(G)$  into  $\Theta^*$ -classes  $F_1, \dots, F_k$ , which are called cuts. These cuts dissect the given graph into two or more connected convex components in order to determine the corresponding descriptor of the compound [33–35, 45]. A coarser partition  $\Theta^{c*}$  is a partition  $\{E_1, \dots, E_p\}$  in which each set  $E_i$  is the union of one or more  $\Theta^*$ -classes of  $G$ . The formulae for determining the topological indices using this technique is summarized in the following theorem.

**Theorem 1.** [31–33] Let  $G_{sw} = (G, (w_v, s_v), (w_e, s_e))$  be a strength-weighted graph. Let  $\mathcal{E}(G) = \{E_1, E_2, \dots, E_p\}$  be a  $\Theta^{c*}$ -partition of  $E(G)$ , and  $TI \in \{W, W_e, W_{ev}, Sz_v, Sz_e, Sz_{ev}, PI, S, Gut, Mo, Mo_e, Mo_t, w^+Mo, w^+Mo_e, w^+Mo_t, w^*Mo, w^*Mo_e, w^*Mo_t\}$ . Then,

$$TI(G_{sw}) = \sum_{i=1}^p TI(G/E_i, (w_v^i, s_v^i), (w_e^i, s_e^i)),$$

where

- (i)  $w_v^i : V(G_{sw}/E_i) \rightarrow \mathbb{R}_0^+$ ,  $w_v^i(X) = \sum_{x \in V(X)} w_v(x)$ ,  $\forall X \in V(G_{sw}/E_i)$ ,
- (ii)  $s_v^i : V(G_{sw}/E_i) \rightarrow \mathbb{R}_0^+$ ,  $s_v^i(X) = \sum_{xy \in E(X)} s_e(xy) + \sum_{x \in V(X)} s_v(x)$ ,  $\forall X \in V(G_{sw}/E_i)$ ,
- (iii)  $w_e^i : E(G_{sw}/E_i) \rightarrow \mathbb{R}_0^+$ ,  $w_e^i(XY) = \sum_{\substack{xy \in E_i \\ x \in V(X), y \in V(Y)}} w_e(xy)$ ,  $\forall XY \in E(G_{sw}/E_i)$ ,

where we apply

- if  $TI \in \{w^+Mo, w^+Mo_e, w^+Mo_t\}$ ,  $w_e^i(XY) = w_e^{+i}(XY) = \sum_{\substack{xy \in E_i \\ x \in V(X), y \in V(Y)}} (d_{G_{sw}}(x) + d_{G_{sw}}(y))$ ,  
 $\forall XY \in E(G_{sw}/E_i)$ ,
- if  $TI \in \{w^*Mo, w^*Mo_e, w^*Mo_t\}$ ,  $w_e^i(XY) = w_e^{*i}(XY) = \sum_{\substack{xy \in E_i \\ x \in V(X), y \in V(Y)}} d_{G_{sw}}(x)d_{G_{sw}}(y)$ ,  
 $\forall XY \in E(G_{sw}/E_i)$ .
- if  $TI$  is other than the above indices,  $w_e^i$  is not needed.

$$(iv) \quad s_e^i : E(G_{sw}/E_i) \rightarrow \mathbb{R}_0^+, \quad s_e^i(XY) = \sum_{\substack{xy \in E_i \\ x \in V(X), y \in V(Y)}} s_e(xy), \quad \forall XY \in E(G_{sw}/E_i).$$

### 3 Molybdenum and Tungsten Disulfides

As we noted in the introduction, molybdenum and tungsten disulfides are novel quasi-two-dimensional transition metal disulfides with excellent physico-chemical properties complementary to those of semimetallic graphene [48], promising several potential applications [4, 18]. These are layered semiconductor materials of the form S–M–S, in which each plane of the metal (M) atoms are sandwiched between two layers of sulfur (S) atoms. Here the bonding within each sandwich layer is strongly covalent while the individual S–M–S layers are loosely held through van der Waals interaction, which thus facilitates the exfoliation of a single layer to a few layers from the bulk [3, 17].

The two popular crystal phases for the bulk  $\text{MoS}_2$  and  $\text{WS}_2$  structures are: (i) a thermodynamically stable 2H phase (hexagonal symmetry) with the  $P63/mmc$  space group [49] (ii) a metastable 1T phase (trigonal symmetry) with the  $P\bar{3}m1$  space group [50] which are characterized by trigonal prismatic and octahedral coordination of metal atoms, respectively as shown in Figure 1. As these phases of  $\text{MS}_2$  monolayers exhibit substantially different electronic properties (for example, 2H  $\text{MoS}_2$  is a semiconductor whereas 1T  $\text{MoS}_2$  is metallic [51]), the characterization of the structure in these phases is efficacious.

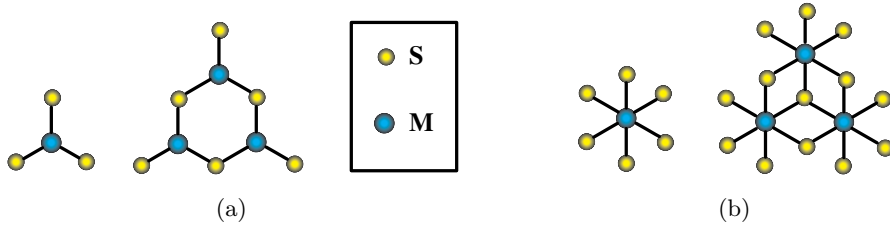


Figure 1: Unit cells and monolayers of  $\text{MS}_2$  in (a) 2H phase (b) 1T phase

We apply relativistic topological models for the characterization of  $\text{MoS}_2$  and  $\text{WS}_2$  as relativistic effects including spin-orbit coupling are significant for such heavy transition metal atoms and main

group atoms as Mo, W, Sn, Pd and so on [19–21, 52–54]. Both scalar relativistic effects such as mass-velocity and Darwin corrections as well as 2-component spinor based spin-orbit coupling are quite significant. As shown in ref [21], even the ground state of tungsten atom is completely altered by spin-orbit effects compared to Cr and Mo which tend to have  $(n - 1)d^5ns^1$  ground states while W exhibits a  $5d^46s^2$  ground state with a large spin-orbit splitting of over  $6200\text{ cm}^{-1}$  or  $0.77\text{ eV}$  [20, 21]. These large spin-orbit effects manifest themselves in the optical, trion, excitonic properties and spin valley dynamics of WS<sub>2</sub>, all of which are attributed to the large spin-orbit splitting of W. Moreover such effects modify the topography of the potential energy surfaces of these systems as shown in refs [19–21, 52–54].

Consequently, it is of paramount importance to quantify these relativistic effects in any realistic topological characterization of their 2D molecular structures. Such realistic parameters for the materials under consideration can be obtained through a localization of relativistically obtained Bloch orbitals into Wannier functions by localized transformations such as the efficient Pipek-Mezey transformation [55]. Hence we introduce relativistic weights  $\gamma_M$  for the metal atom,  $\gamma_S$  for the sulfur atom and  $\rho_{MS}$  for each edge M–S in the 2D network of MoS<sub>2</sub> and WS<sub>2</sub>. We now traverse the relativistic structural attributes of two phases of MS<sub>2</sub> (M = Mo, W) by analyzing their molecular model in various forms depending on the arrangement of the corresponding unit cells [56–59].

### 3.1 Mathematical Key Idea

The key idea of this paper is to correctly locate the  $\Theta$ -classes of 2H MS<sub>2</sub> and 1T MS<sub>2</sub> monolayers from their underlying graph structures. That is, we are going to show that the graph structures of 2H MS<sub>2</sub> and 1T MS<sub>2</sub> monolayers belong to the family of partial cubes.

The graph structure of 2H MS<sub>2</sub> monolayer can be easily constructed from benzenoid systems by attaching pendant edges in specific places on the boundaries as shown in Figure 2. That benzenoid systems are partial cubes is known already from the seminal paper [60] in which the cut method was introduced. Moreover, it is clear (and well-known) that attaching pendant edges to partial cubes yields partial cubes again. Hence we can conclude that the graph structure of 2H MS<sub>2</sub> monolayers are partial cubes. The graph structure of 1T MS<sub>2</sub> monolayers can be constructed from 2H MS<sub>2</sub> graph structure by adding vertices and edges as shown in the right-hand side of Figure 2. To prove that 1T MS<sub>2</sub> graph structures are partial cubes, we need some preparation.

Let  $G$  be a graph and let  $W_1, W_2 \subseteq V(G)$  be vertex subsets that cover  $V(G)$  and have nonempty intersection, that is,  $W_1 \cup W_2 = V(G)$  and  $W_1 \cap W_2 \neq \emptyset$ . Assume further that the subgraphs induced by  $W_1$  and by  $W_2$  are isometric in  $G$ , as well as that there are no edges between  $W_1 \setminus W_2$  and  $W_2 \setminus W_1$ . Under these assumptions, let  $H$  be a graph constructed as follows.

- Replace each vertex  $w \in W_1 \cap W_2$  by vertices  $w_1$  and  $w_2$  and add the edge  $w_1w_2$ .
- Join  $w_1$  and  $w_2$  to all neighbors of  $w$  in  $W_1 \setminus W_2$  and  $W_2 \setminus W_1$ , respectively.
- If  $w, z \in W_1 \cap W_2$  and  $wz \in E(G)$ , then add edges  $w_1z_1$  and  $w_2z_2$ .

Then we say that  $H$  is an *expansion of  $G$  with respect to  $W_1, W_2$* . In addition, a *contraction* is the inverse operation of the expansion, that is, we say that in the above construction  $G$  is a *contraction of  $H$* . Finally, an *expansion procedure* is a sequence of expansions. With this preparation we can now state the following characterization of partial cubes due to Chepoi [61].

**Theorem 2.** *A graph  $G$  is a partial cube if and only if  $G$  can be obtained from the one vertex graph  $K_1$  by a sequence of expansions.*

Using Theorem 2 we can now deduce the following.

**Theorem 3.** *The graph structures of 1T  $MS_2$  monolayers are partial cubes.*

*Proof.* It is enough to prove that the graph structure of 1T  $MS_2$  without pendant edges are partial cubes. We now construct the 1T  $MS_2$  monolayers without pendant edges as shown in Figure 3. First contract the “ladder” subgraph as shown in the Figure 3. Note that the bottom marked path is isometric in the graph, as well as it is the upper marked path, hence by Theorem 2, the left top graph is a partial cube if and only if the top right graph is a partial cube.

We then proceed analogously by contracting horizontal isometric paths from top to bottom. See Figure 3 again, where the next two steps of the contraction are presented. Continuing in this manner we end up with a grid-like graph  $H$ . By the same method (but simpler) we see that  $H$  is a partial cube. More precisely, we contract diagonal ladder subgraphs from, say, top left till bottom right. We conclude that since  $H$  is a partial cube, then so it is the starting 1T  $MS_2$  monolayer.  $\square$

### 3.2 2H $MS_2$ monolayers

In the 2H phase, each metal atom  $M$  is prismatically coordinated by three surrounding sulfur atoms  $S$ , with the  $S$  atoms in the upper layer lying directly above those of the lower layer. The grain boundaries of these 2H monolayer  $MS_2$  possess significant impact in the electronic, magnetic and transport properties of the compounds [62, 63]. The schematic representation of the two types of 2H  $MS_2$  monolayers [56, 57] are depicted in Figure 4. The bitrapezium, hexagonal and parallelogram shapes of 2H  $MS_2$  monolayers are respectively denoted by  $BT_H(n, p, q)$ ,  $H_H(k)$ , and  $P_H(p, q)$ . Since the hexagonal shape is a particular case of bitrapezium, the relativistic topological indices can easily deduced from that bitrapezium shape.

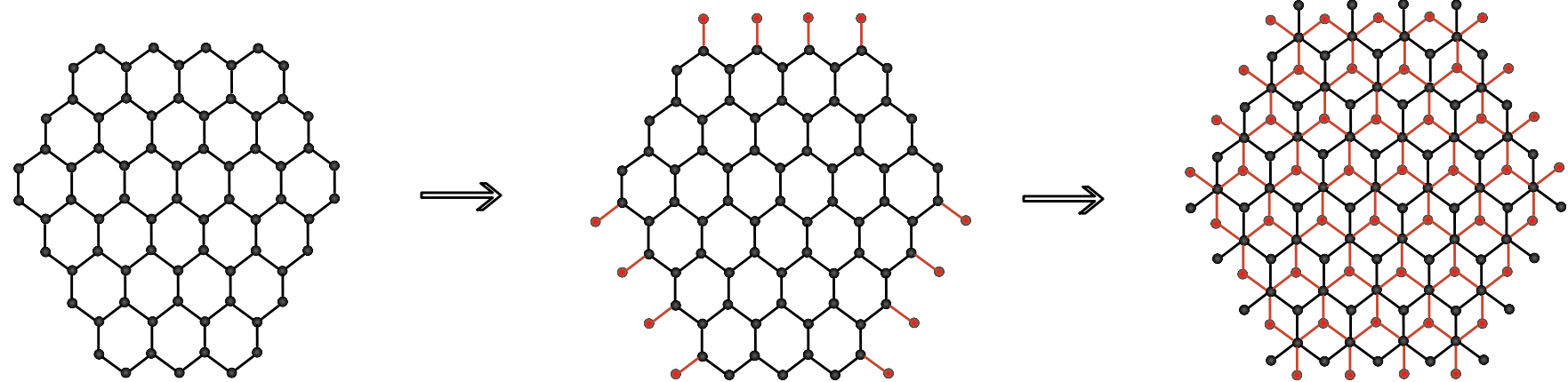


Figure 2: Construction of  $\text{MoS}_2$  monolayers from benzenoid systems

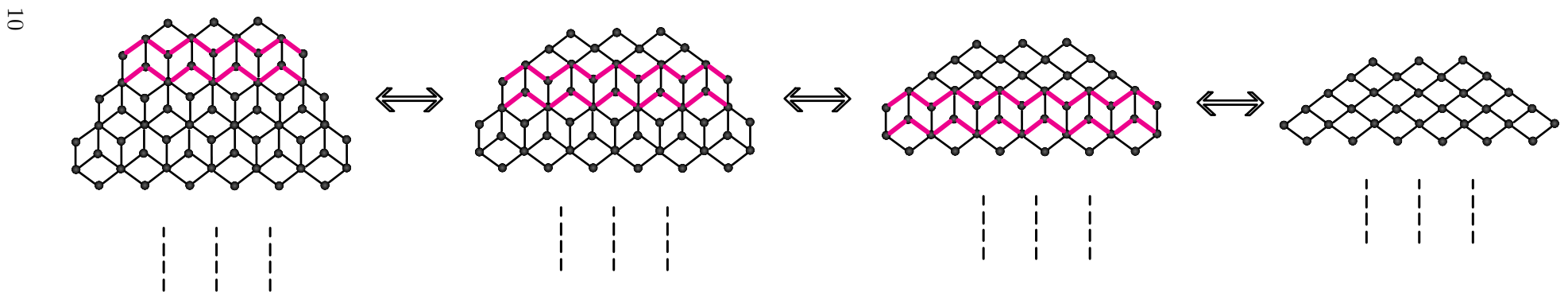


Figure 3: Various stages of 1T  $\text{MS}_2$  monolayer by contraction procedure

The  $\Theta$ -classes of these structures are grouped into four categories as horizontal  $H_{\pm i}^{H\#}$ , acute  $A_{\pm i}^{H\#}$ , obtuse  $O_{\pm i}^{H\#}$  and pendant  $P_i^{H\#}$  as depicted in Figure 5, where  $\# \in \{b, h, p\}$  denotes the geometry of the structure and  $i \in I$ , the index set of  $\Theta$ -classes. The quotient graph of all  $\Theta$ -classes is a complete graph on two vertices with the vertex strength-weights  $(X_{ki}^{H\#}(w), X_{ki}^{H\#}(s))$ ,  $k = 1, 2$  and edge strength-weights as  $(X_{3i}^{H\#}(w^+)/X_{3i}^{H\#}(w^*), X_{3i}^{H\#}(s))$ ,  $X \in \{H, A, O, P\}$  as in Figure 6.

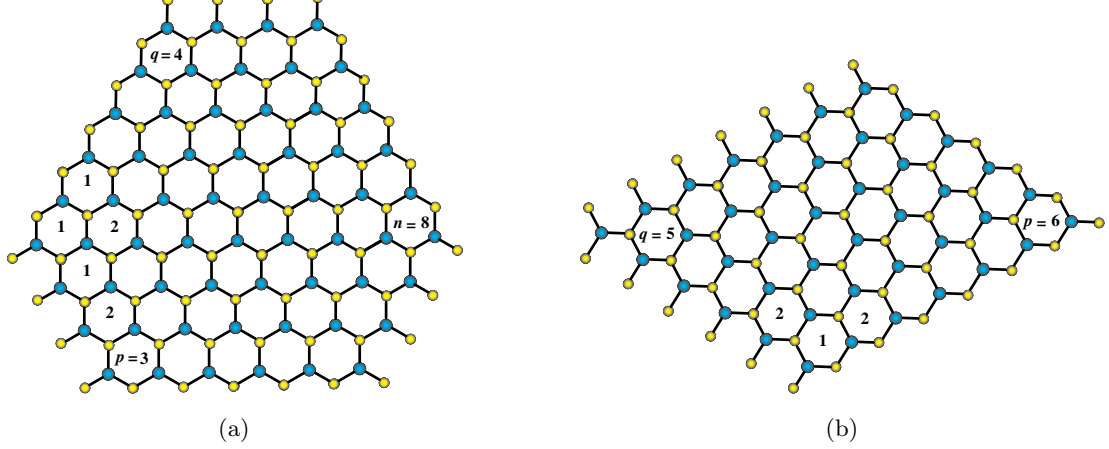


Figure 4: Structure of 2H MS<sub>2</sub> monolayers (a)  $BT_H(8,3,4)$  (b)  $P_H(6,5)$

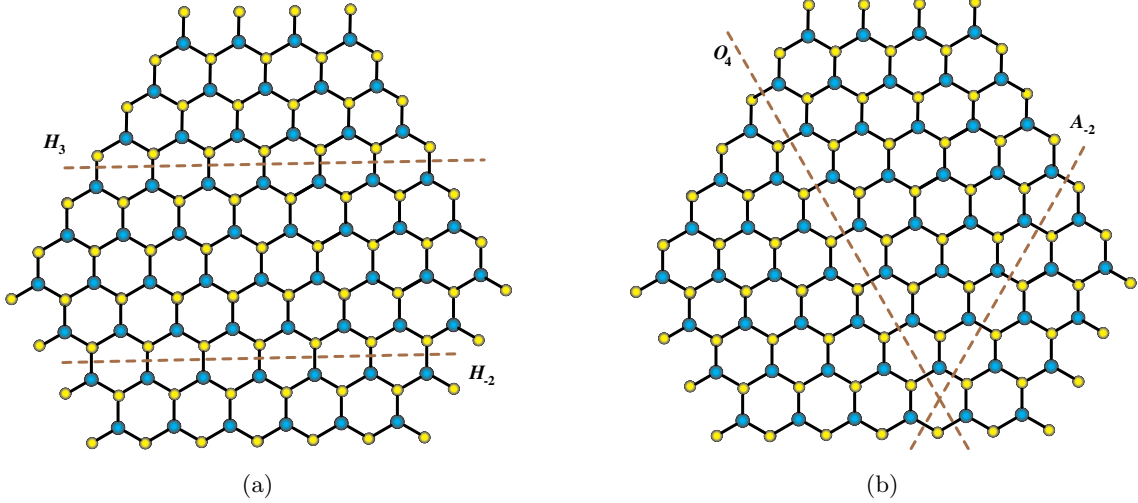


Figure 5: Various  $\Theta$ -classes of  $BT_H(8,3,4)$

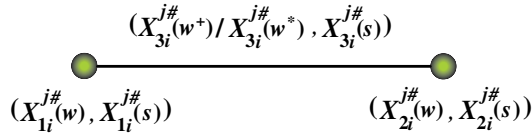


Figure 6: Quotient graph of  $\Theta$ -class where  $j \in \{H, T\}$

**Theorem 4.** For bitrapezium shape 2H MS<sub>2</sub> monolayer BT<sub>H</sub>(n, p, q), p + q ≤ n, we have

1.  $W(BT_H(n, p, q)) = \frac{1}{60}\{\gamma_s^2(20n^3p^2 + 40n^3pq + 120n^3p + 20n^3q^2 + 120n^3q + 180n^3 - 20n^2p^3 + 90n^2p^2 + 240n^2pq + 710n^2p - 20n^2q^3 - 30n^2q^2 + 350n^2q + 840n^2 + 10np^4 - 60np^3 + 120np^2 + 440npq + 1290np + 10nq^4 + 20nq^3 + 370nq + 1140n - 4p^5 - 10p^4q - 15p^4 - 20p^3q - 90p^3 + 10p^2q + 195p^2 - 10pq^4 - 100pq^3 - 350pq^2 - 240pq + 634p - 4q^5 - 35q^4 - 170q^3 - 385q^2 - 246q + 360) + \gamma_M^2(20n^3p^2 + 40n^3pq + 80n^3p + 20n^3q^2 + 80n^3q + 80n^3 - 20n^2p^3 + 30n^2p^2 + 120n^2pq + 230n^2p - 20n^2q^3 - 30n^2q^2 + 110n^2q + 180n^2 + 10np^4 - 20np^3 + 80npq + 150np + 10nq^4 + 20nq^3 + 50nq + 100n - 4p^5 - 10p^4q - 15p^4 - 20p^3q - 30p^3 + 10p^2q + 15p^2 - 10pq^4 - 60pq^3 - 110pq^2 - 40pq + 34p - 4q^5 - 25q^4 - 70q^3 - 95q^2 - 46q) + \gamma_M\gamma_s(40n^3p^2 + 80n^3pq + 200n^3p + 40n^3q^2 + 200n^3q + 240n^3 - 40n^2p^3 + 120n^2p^2 + 360n^2pq + 880n^2p - 40n^2q^3 - 60n^2q^2 + 460n^2q + 840n^2 + 20np^4 - 80np^3 + 90np^2 + 460npq + 1110np + 20nq^4 + 40nq^3 - 30nq^2 + 390nq + 900n - 8p^5 - 20p^4q - 30p^4 - 40p^3q - 130p^3 + 20p^2q + 30p^2 - 20pq^4 - 160pq^3 - 430pq^2 - 250pq + 318p - 8q^5 - 60q^4 - 220q^3 - 450q^2 - 282q + 180)\}.$
2.  $W_e(BT_H(n, p, q)) = \frac{3}{40}\rho_{MS}^2\{40n^3p^2 + 80n^3pq + 160n^3p + 40n^3q^2 + 160n^3q + 160n^3 - 40n^2p^3 + 120n^2pq + 240n^2p - 40n^2q^3 - 120n^2q^2 + 160n^2 + 20np^4 + 20np^3 + 60np^2q + 80np^2 + 60npq^2 + 240npq + 240np + 20nq^4 + 100nq^3 + 200nq^2 + 240nq + 160n - 8p^5 - 20p^4q - 45p^4 - 40p^3q - 50p^3 - 30p^2q^2 - 50p^2q + 5p^2 - 20pq^4 - 120pq^3 - 230pq^2 - 130pq + 18p - 8q^5 - 65q^4 - 190q^3 - 235q^2 - 102q\}.$
3.  $W_{ev}(BT_H(n, p, q)) = \frac{1}{80}\rho_{MS}\{\gamma_M(360n + 86p - 194q + 520n^2 + 320n^3 + 35p^2 - 110p^3 - 75p^4 - 16p^5 - 425q^2 - 330q^3 - 115q^4 - 16q^5 + 80np^2 + 700n^2p - 20np^3 + 320n^3p + 40np^4 + 200nq^2 + 220n^2q + 140nq^3 + 320n^3q + 40nq^4 - 450pq^2 - 30p^2q - 240pq^3 - 80p^3q - 40pq^4 - 40p^4q + 60n^2p^2 - 80n^2p^3 + 80n^3p^2 - 180n^2q^2 - 80n^2q^3 + 80n^3q^2 - 30p^2q^2 + 540np + 340nq - 210pq + 400npq + 60npq^2 + 60np^2q + 360n^2pq + 160n^3pq) + \gamma_s(240 + 1400n + 526p - 474q + 1360n^2 + 480n^3 + 135p^2 - 210p^3 - 75p^4 - 16p^5 - 845q^2 - 490q^3 - 135q^4 - 16q^5 + 220np^2 + 1460n^2p - 100np^3 + 400n^3p + 40np^4 + 180nq^2 + 620n^2q + 140nq^3 + 400n^3q + 40nq^4 - 830pq^2 - 30p^2q - 320pq^3 - 80p^3q - 40pq^4 - 40p^4q + 180n^2p^2 - 80n^2p^3 + 80n^3p^2 - 180n^2q^2 - 80n^2q^3 + 80n^3q^2 - 30p^2q^2 + 1840np + 760nq - 510pq + 920npq + 60npq^2 + 60np^2q + 600n^2pq + 160n^3pq)\}.$
4.  $Sz_v(BT_H(n, p, q)) = \frac{1}{240}\rho_{MS}\{\gamma_M^2(120n^3p^3 + 360n^3p^2q + 720n^3p^2 + 360n^3pq^2 + 1440n^3pq + 1400n^3p + 120n^3q^3 + 720n^3q^2 + 1400n^3q + 880n^3 - 180n^2p^4 - 360n^2p^3q - 560n^2p^3 - 360n^2p^2q^2 - 600n^2p^2q + 300n^2p^2 - 360n^2pq^3 - 840n^2pq^2 + 840n^2pq + 2120n^2p - 180n^2q^4 - 880n^2q^3 - 900n^2q^2 + 1000n^2q + 1440n^2 + 90np^5 + 90np^4q - 20np^4 + 180np^3q^2 - 120np^3q - 1010np^3 + 180np^2q^3 + 360np^2q^2 - 630np^2q - 1180np^2 + 90npq^4 + 120npq^3 - 390npq^2 - 360npq + 360np + 90nq^5 + 380nq^4 + 190nq^3 - 620nq^2 - 120nq + 560n - 15p^6 + 73p^5 - 45p^4q^2 + 75p^4q + 345p^4 + 110p^3q^2 + 430p^3q + 335p^3 - 45p^2q^4 - 110p^2q^3 + 270p^2q^2 + 695p^2q + 150p^2 - 75pq^4 - 370pq^3 - 455pq^2 + 72p - 15q^6 - 73q^5 - 135q^4 -$

$$\begin{aligned}
& 255q^3 - 450q^2 - 272q) + \gamma_s^2(120n^3p^3 + 360n^3p^2q + 1000n^3p^2 + 360n^3pq^2 + 2000n^3pq + 2480n^3p + \\
& 120n^3q^3 + 1000n^3q^2 + 2480n^3q + 1920n^3 - 180n^2p^4 - 360n^2p^3q - 480n^2p^3 - 360n^2p^2q^2 - 240n^2p^2q + \\
& 2340n^2p^2 - 360n^2pq^3 - 840n^2pq^2 + 4080n^2pq + 8400n^2p - 180n^2q^4 - 1160n^2q^3 - 660n^2q^2 + 5120n^2q + \\
& 6720n^2 + 90np^5 + 90np^4q - 330np^4 + 180np^3q^2 - 480np^3q - 2670np^3 + 180np^2q^3 + 180np^2q^2 - \\
& 1650np^2q - 1870np^2 + 90npq^4 - 240npq^3 - 2490npq^2 + 460npq + 6700np + 90nq^5 + 430nq^4 - 790nq^3 - \\
& 3470nq^2 + 1100nq + 6480n - 15p^6 + 179p^5 - 45p^4q^2 + 115p^4q + 565p^4 + 290p^3q^2 + 610p^3q - 515p^3 - \\
& 45p^2q^4 - 110p^2q^3 + 570p^2q^2 + 715p^2q - 910p^2 + 55pq^4 - 150pq^3 - 1785pq^2 - 1660pq + 1416p - 15q^6 - \\
& 57q^5 + 185q^4 - 15q^3 - 2210q^2 - 1968q + 1440) + \gamma_M\gamma_s(240n^3p^3 + 720n^3p^2q + 1720n^3p^2 + 720n^3pq^2 + \\
& 3440n^3pq + 3800n^3p + 240n^3q^3 + 1720n^3q^2 + 3800n^3q + 2640n^3 - 360n^2p^4 - 720n^2p^3q - 1040n^2p^3 - \\
& 720n^2p^2q^2 - 840n^2p^2q + 2280n^2p^2 - 720n^2pq^3 - 1680n^2pq^2 + 4440n^2pq + 9200n^2p - 360n^2q^4 - \\
& 2040n^2q^3 - 1680n^2q^2 + 5280n^2q + 6720n^2 + 180np^5 + 180np^4q - 350np^4 + 360np^3q^2 - 600np^3q - \\
& 3600np^3 + 360np^2q^3 + 540np^2q^2 - 2280np^2q - 3290np^2 + 180npq^4 - 120npq^3 - 2400npq^2 - 140npq + \\
& 4900np + 180nq^5 + 810nq^4 - 360nq^3 - 3370nq^2 + 820nq + 5040n - 30p^6 + 252p^5 - 90p^4q^2 + 190p^4q + \\
& 970p^4 + 400p^3q^2 + 1040p^3q + 140p^3 - 90p^2q^4 - 220p^2q^3 + 840p^2q^2 + 1410p^2q - 820p^2 - 20pq^4 - \\
& 680pq^3 - 2120pq^2 - 1380pq + 448p - 30q^6 - 130q^5 - 50q^4 - 470q^3 - 2440q^2 - 1920q + 720).
\end{aligned}$$

$$5. Sz_e(BT_H(n, p, q)) = \frac{1}{80}\rho_{MS}^3\{360n^3p^3 + 1080n^3p^2q + 2040n^3p^2 + 1080n^3pq^2 + 4080n^3pq + 3840n^3p + \\
360n^3q^3 + 2040n^3q^2 + 3840n^3q + 2400n^3 - 540n^2p^4 - 1080n^2p^3q - 1720n^2p^3 - 1080n^2p^2q^2 - \\
2280n^2p^2q - 420n^2p^2 - 1080n^2pq^3 - 3120n^2pq^2 - 480n^2pq + 2920n^2p - 540n^2q^4 - 2720n^2q^3 - \\
3900n^2q^2 - 280n^2q + 1920n^2 + 270np^5 + 270np^4q + 140np^4 + 540np^3q^2 + 360np^3q - 1270np^3 + \\
540np^2q^3 + 1680np^2q^2 + 750np^2q - 980np^2 + 270npq^4 + 840npq^3 + 1110npq^2 + 1800npq + 1600np + \\
270nq^5 + 1300nq^4 + 1970nq^3 + 1340nq^2 + 1600nq + 1440n - 45p^6 + 131p^5 - 135p^4q^2 - 15p^4q + \\
445p^4 + 130p^3q^2 + 450p^3q + 345p^3 - 135p^2q^4 - 490p^2q^3 - 330p^2q^2 + 145p^2q - 160p^2 - 225pq^4 - \\
1270pq^3 - 2185pq^2 - 1220pq - 236p - 45q^6 - 251q^5 - 695q^4 - 1465q^3 - 1900q^2 - 924q\}.$$

$$6. Sz_{ev}(BT_H(n, p, q)) = \frac{1}{240}\rho_{MS}^2\{\gamma_M(1560n - 10p - 870q + 3120n^2 + 2520n^3 + 145p^2 + 675p^3 + 740p^4 + \\
175p^5 - 45p^6 - 1625q^2 - 1115q^3 - 550q^4 - 235q^5 - 45q^6 - 2260np^2 + 4640n^2p - 2150np^3 + 4020n^3p + \\
40np^4 + 270np^5 - 260nq^2 + 1360n^2q + 1270nq^3 + 4020n^3q + 1220nq^4 + 270nq^5 - 1775pq^2 + 1115p^2q - \\
1190pq^3 + 870p^3q - 225pq^4 + 105p^4q + 240n^2p^2 - 1700n^2p^3 + 2100n^3p^2 - 540n^2p^4 + 360n^3p^3 - \\
3300n^2q^2 - 2680n^2q^3 + 2100n^3q^2 - 540n^2q^4 + 360n^3q^3 + 240p^2q^2 - 410p^2q^3 + 230p^3q^2 - 135p^2q^4 - \\
135p^4q^2 + 1340np + 620nq - 610pq + 360npq - 1080n^2p^2q^2 - 30npq^2 - 570np^2q + 1020n^2pq + \\
600npq^3 + 4200n^3pq + 270npq^4 + 270np^4q + 1380np^2q^2 - 2820n^2pq^2 - 2040n^2p^2q + 540np^2q^3 + \\
540np^3q^2 - 1080n^2pq^3 - 1080n^2p^3q + 1080n^3pq^2 + 1080n^3p^2q) + \gamma_s(720 + 5520n + 766p - 2094q + \\
8040n^2 + 3720n^3 - 345p^2 + 460p^3 + 1230p^4 + 334p^5 - 45p^6 - 2765q^2 - 635q^3 - 130q^4 - 211q^5 - \\
45q^6 - 4195np^2 + 11300n^2p - 4560np^3 + 5400n^3p - 425np^4 + 270np^5 - 3635nq^2 + 5620n^2q + 40nq^3 +
\]$$

$$5400n^3q + 1295nq^4 + 270nq^5 - 2510pq^2 + 1865p^2q - 860pq^3 + 1300p^3q - 30pq^4 + 165p^4q + 2700n^2p^2 - 1580n^2p^3 + 2520n^3p^2 - 540n^2p^4 + 360n^3p^3 - 3060n^2q^2 - 3100n^2q^3 + 2520n^3q^2 - 540n^2q^4 + 360n^3q^3 + 930p^2q^2 - 410p^2q^3 + 500p^3q^2 - 135p^2q^4 - 135p^4q^2 + 5430np + 710nq - 1520pq - 210npq - 1080n^2p^2q^2 - 2700npq^2 - 2340np^2q + 4920n^2pq + 60npq^3 - 540np^3q + 5040n^3pq + 270npq^4 + 270np^4q + 1110np^2q^2 - 2820n^2pq^2 - 1500n^2p^2q + 540np^2q^3 + 540np^3q^2 - 1080n^2pq^3 - 1080n^2p^3q + 1080n^3pq^2 + 1080n^3p^2q\}.$$

7.  $PI(BT_H(n, p, q)) = \frac{1}{4}\rho_{MS}^2\{36n^2p^2 + 72n^2pq + 140n^2p + 36n^2q^2 + 140n^2q + 140n^2 - 36np^3 - 36np^2q - 40np^2 - 36npq^2 - 16npq + 108np - 36nq^3 - 112nq^2 - 36nq + 100n + 9p^4 - 14p^3 + 18p^2q^2 + 26p^2q - 5p^2 - 10pq^2 - 2pq + 42p + 9q^4 + 22q^3 - 5q^2 - 18q + 24\}.$
8.  $S(BT_H(n, p, q)) = \frac{1}{10}\rho_{MS}\{\gamma_M(30 + 300n + 73p - 127q + 380n^2 + 160n^3 - 5p^2 - 70p^3 - 30p^4 - 8p^5 - 235q^2 - 150q^3 - 50q^4 - 8q^5 + 10np^2 + 470n^2p - 40np^3 + 160n^3p + 20np^4 + 10nq^2 + 230n^2q + 40nq^3 + 160n^3q + 20nq^4 - 240pq^2 - 120pq^3 - 40p^3q - 20pq^4 - 20p^4q + 60n^2p^2 - 40n^2p^3 + 40n^3p^2 - 60n^2q^2 - 40n^2q^3 + 40n^3q^2 + 390np + 170nq - 120pq + 200npq + 240n^2pq + 80n^3pq) + \gamma_S(210 + 970n + 353p - 297q + 860n^2 + 240n^3 + 30p^2 - 135p^3 - 30p^4 - 8p^5 - 475q^2 - 230q^3 - 60q^4 - 8q^5 + 95np^2 + 880n^2p - 80np^3 + 200n^3p + 20np^4 - 15nq^2 + 460n^2q + 40nq^3 + 200n^3q + 20nq^4 - 445pq^2 - 160pq^3 - 40p^3q - 20pq^4 - 20p^4q + 120n^2p^2 - 40n^2p^3 + 40n^3p^2 - 60n^2q^2 - 40n^2q^3 + 40n^3q^2 + 1175np + 425nq - 285pq + 490npq + 360n^2pq + 80n^3pq)\}.$
9.  $Gut(BT_H(n, p, q)) = \frac{1}{10}\rho_{MS}^2\{120n^3p^2 + 240n^3pq + 480n^3p + 120n^3q^2 + 480n^3q + 480n^3 - 120n^2p^3 + 180n^2p^2 + 720n^2pq + 1430n^2p - 120n^2q^3 - 180n^2q^2 + 710n^2q + 1190n^2 + 60np^4 - 120np^3 + 50np^2 + 680npq + 1350np + 60nq^4 + 120nq^3 + 50nq^2 + 630nq + 1090n - 24p^5 - 60p^4q - 90p^4 - 120p^3q - 230p^3 - 40p^2q - 65p^2 - 60pq^4 - 360pq^3 - 760pq^2 - 440pq + 249p - 24q^5 - 150q^4 - 470q^3 - 785q^2 - 441q + 150\}.$

*Proof.* The cardinality of structural vertex set and the edge set of  $BT_H(n, p, q)$  is given by  $|V_\gamma(BT_H(n, p, q))| = (\gamma_M(2 + 4n + p - q - p^2 - q^2 + 2np + 2nq) + \gamma_S(6 + 6n + 3p - q - p^2 - q^2 + 2np + 2nq))/2$  and  $|E_\rho(BT_H(n, p, q))| = 3\rho_{MS}(4n + p - q + 2np + 2nq - p^2 - q^2 + 2)/2$  while the total number of vertices and edges in the underlying graph are  $5n + 2p - q + 2np + 2nq - p^2 - q^2 + 4$  and  $3(4n + p - q + 2np + 2nq - p^2 - q^2 + 2)/2$  respectively.

As the  $\Theta$ -classes  $A_{\pm i}^{hb}$  and  $O_{\pm i}^{hb}$  are symmetric to each other in  $BT_H(n, p, q)$ , it is sufficient to determine the strength-weighted parameters for the three types of  $\Theta$ -classes. The computed values of the strength-weighted parameters of the quotient graphs are tabulated in Table 2 and in addition that  $X_{2i}^{hb}(w) = |V_\gamma(BT_H(n, p, q))| - X_{1i}^{hb}(w)$  and  $X_{2i}^{hb}(s) = |E_\rho(BT_H(n, p, q))| - X_{1i}^{hb}(s) - X_{3i}^{hb}(s)$ . We thus evaluate the various indices  $TI \in \{W, W_e, W_{ev}, Sz_v, Sz_e, Sz_{ev}, PI, S, Gut\}$  by substituting the above mentioned parameter values in the following expression,

$$TI(BT_H(n, p, q)) = \sum_{i=1}^{q+1} TI(BT_H(n, p, q)/H_i^{hb}) + \sum_{i=1}^p TI(BT_H(n, p, q)/H_{-i}^{hb})$$

$$\begin{aligned}
& + 2 \sum_{i=1}^p TI(BT_H(n, p, q)/A_i^{Hb}) + 2 \sum_{i=p+1}^{n-q} TI(BT_H(n, p, q)/A_i^{Hb}) \\
& + 2 \sum_{i=1}^q TI(BT_H(n, p, q)/A_{-i}^{Hb}) + \sum_{i=1}^{n-q+2(p+1)} TI(BT_H(n, p, q)/P_i^{Hb}).
\end{aligned}$$

Table 2: Strength-weighted parameters of  $BT_H(n, p, q)$

| $\Theta$ -class                      | Edge-strength $X_{3i}^{Hb}(s)$ | Vertex-weight $X_{1i}^{Hb}(w)$                                | Vertex-strength $X_{1i}^{Hb}(s)$        |
|--------------------------------------|--------------------------------|---|---|
| $H_i^{Hb}: 1 \leq i \leq q+1$        | $\rho_{MS}(n - q + i)$         | $(\gamma_s(i+1)(i+2n-2q) + i\gamma_M(i+2n-2q-1))/2$           | $3i\rho_{MS}(i+2n-2q-1)/2$              |
| $H_{-i}^{Hb}: 1 \leq i \leq p$       | $\rho_{MS}(n - p + i)$         | $(i\gamma_M(i+2n-2p+1) + i\gamma_s(i+2n-2p+3))/2$             | $\rho_{MS}(i-2n+2p+6ni-6ip+3i^2)/2$     |
| $A_i^{Hb}: 1 \leq i \leq p$          | $\rho_{MS}(q+i+1)$             | $(i\gamma_s(i+2q+5) + i\gamma_M(i+2q+3))/2$                   | $\rho_{MS}(7i-2q+6iq+3i^2-2)/2$         |
| $A_i^{Hb}: p+1 \leq i \leq n-q$      | $\rho_{MS}(p+q+2)$             | $(\gamma_s(6i-p-p^2+2ip+2iq) + \gamma_M(4i-p-p^2+2ip+2iq))/2$ | $\rho_{MS}(12i-5p-2q+6ip+6iq-3p^2-4)/2$ |
| $A_{-i}^{Hb}: 1 \leq i \leq q$       | $\rho_{MS}(p+i+1)$             | $(\gamma_s(2(p+1) + i(i+2p+3)) + i\gamma_M(i+2p+1))/2$        | $3i\rho_{MS}(i+2p+1)/2$                 |
| $P_i^{Hb}: 1 \leq i \leq n-q+2(p+1)$ | $\rho_{MS}$                    | $\gamma_s$  | 0                                       |

□

It should be noted that the geometry of the bitrapezium graph structure  $BT_H(n, p, q)$  possess complications in MATLAB interface while calculating the Mostar indices. Thus we limit the evaluation of various Mostar indices to the hexagonal shape  $MS_2$  monolayer. Since  $H_H(k) = BT_H(2k-1, k-1, k-1)$  and consequently, all the other indices namely  $W, W_e, W_{ev}, Sz_v, Sz_e, Sz_{ev}, PI, S, Gut$  for this structure can be obtained from Theorem 4 by replacing the values of the parameters  $n, p$  and  $q$  as  $2k-1, k-1$  and  $k-1$  respectively.

**Theorem 5.** For hexagonal shape  $2H$   $MS_2$  monolayer  $H_H(k)$ , we have

1.  $Mo(H_H(k)) = \frac{1}{2}k\rho_{MS}\{\gamma_M(27k^3 + 3k) + \gamma_s(27k^3 + 16k^2 - 3k - 16)\}.$
2.  $Mo_e(H_H(k)) = \frac{3}{2}k\rho_{MS}^2\{27k^3 - 5k - 2\}.$

3.  $Mo_t(H_H(k)) = \frac{1}{2}k\rho_{MS}\{\rho_{MS}(81k^3 - 15k - 6) + \gamma_M(27k^3 + 3k) + \gamma_S(27k^3 + 16k^2 - 3k - 16)\}.$
4.  $w^+ Mo(H_H(k)) = \frac{1}{5}k\rho_{MS}^2\{\gamma_M(564k^4 - 405k^3 + 330k^2 - 15k + 6) + \gamma_S(564k^4 - 75k^3 - 290k^2 + 135k - 94)\}.$
5.  $w^+ Mo_e(H_H(k)) = \frac{3}{5}k\rho_{MS}^3\{564k^4 - 405k^3 + 90k^2 + 25k - 14\}.$
6.  $w^+ Mo_t(H_H(k)) = \frac{1}{5}k\rho_{MS}^2\{\rho_{MS}(1692k^4 - 1215k^3 + 270k^2 + 75k - 42) + \gamma_M(564k^4 - 405k^3 + 330k^2 - 15k + 6) + \gamma_S(564k^4 - 75k^3 - 290k^2 + 135k - 94)\}.$
7.  $w^* Mo(H_H(k)) = \frac{3}{5}k\rho_{MS}^3\{\gamma_M(282k^4 - 270k^3 + 165k^2 - 15k + 3) + \gamma_S(282k^4 - 105k^3 - 185k^2 + 75k - 7)\}.$
8.  $w^* Mo_e(H_H(k)) = \frac{9}{5}k\rho_{MS}^4\{282k^4 - 270k^3 + 45k^2 + 25k - 2\}.$
9.  $w^* Mo_t(H_H(k)) = \frac{3}{5}k\rho_{MS}^3\{\rho_{MS}(846k^4 - 810k^3 + 135k^2 + 75k - 6) + \gamma_M(282k^4 - 270k^3 + 165k^2 - 15k + 3) + \gamma_S(282k^4 - 105k^3 - 185k^2 + 75k - 7)\}$

*Proof.* Due to the symmetry of the structure  $H_H(k)$ , it is sufficient to estimate the edge-weight parameters for the  $\Theta$ -classes  $H_i^{Hh}$  and  $P_i^{Hh}$ . We have  $H_{\pm 3i}^{Hh}(w^+) = \rho_{MS}(6(k+i) - 2)$ ,  $H_{\pm 3i}^{Hh}(w^*) = \rho_{MS}^2(9(k+i) - 6)$ ,  $P_{3i}^{Hh}(w^+) = 4\rho_{MS}$  and  $P_{3i}^{Hh}(w^*) = 3\rho_{MS}^2$ . Thus we obtain the indices  $TI \in \{Mo, Mo_e, Mo_t, w^+ Mo, w^+ Mo_e, w^+ Mo_t, w^* Mo, w^* Mo_e, w^* Mo_t\}$  by substituting the given values in the following expression,

$$TI(H_H(k)) = 3 \sum_{i=1}^k TI(H_H(k)/H_i^{Hh}) + 3 \sum_{i=1}^{k-1} TI(H_H(k)/H_{-i}^{Hh}) + \sum_{i=1}^{3k} TI(H_H(k)/P_i^{Hh}).$$

□

**Theorem 6.** For parallelogram shape 2H MS<sub>2</sub> monolayer  $P_H(p, q)$ ,  $1 \leq q \leq p$ , we have

1.  $W(P_H(p, q)) = \frac{1}{60}\{\gamma_M^2(20p^3q^2 + 40p^3q + 20p^3 + 10p^2q^3 + 90p^2q^2 + 140p^2q + 60p^2 + 5pq^4 + 40pq^3 + 125pq^2 + 130pq + 40p - q^5 + 25q^3 + 60q^2 + 36q) + \gamma_S^2(20p^3q^2 + 80p^3q + 80p^3 + 10p^2q^3 + 180p^2q^2 + 530p^2q + 480p^2 + 5pq^4 + 80pq^3 + 515pq^2 + 1100pq + 760p - q^5 + 85q^3 + 480q^2 + 756q + 360) + \gamma_M\gamma_S(40p^3q^2 + 120p^3q + 80p^3 + 20p^2q^3 + 270p^2q^2 + 610p^2q + 360p^2 + 10pq^4 + 120pq^3 + 580pq^2 + 930pq + 460p - 2q^5 + 90q^3 + 360q^2 + 452q + 180)\}.$
2.  $W_e(P_H(p, q)) = \frac{1}{20}\rho_{MS}^2(q+1)\{60p^3q + 60p^3 + 30p^2q^2 + 150p^2q + 120p^2 + 15pq^3 + 105pq^2 + 150pq + 60p - 3q^4 + 3q^3 + 62q^2 + 58q\}.$
3.  $W_{ev}(P_H(p, q)) = \frac{1}{60}\rho_{MS}\{\gamma_M(90p + 83q + 150p^2 + 60p^3 + 150q^2 + 70q^3 - 3q^5 + 315pq^2 + 345p^2q + 120pq^3 + 120p^3q + 15pq^4 + 225p^2q^2 + 30p^2q^3 + 60p^3q^2 + 300pq) + \gamma_S(180 + 540p + 533q + 480p^2 + 120p^3 + 480q^2 + 130q^3 - 3q^5 + 750pq^2 + 780p^2q + 180pq^3 + 180p^3q + 15pq^4 + 360p^2q^2 + 30p^2q^3 + 60p^3q^2 + 1095pq)\}.$

4.  $Sz_v(P_H(p, q)) = \frac{1}{60}\rho_{MS}^2\{\gamma_M^2(30p^3q^3 + 90p^3q^2 + 80p^3q + 20p^3 + 90p^2q^3 + 270p^2q^2 + 240p^2q + 60p^2 + 70pq^3 + 210pq^2 + 180pq + 40p + 5q^4 + 30q^3 + 55q^2 + 30q) + \gamma_S^2(30p^3q^3 + 160p^3q^2 + 210p^3q + 80p^3 + 170p^2q^3 + 810p^2q^2 + 1060p^2q + 480p^2 - 5pq^4 + 200pq^3 + 1045pq^2 + 1540pq + 760p + q^5 + 5q^4 + 85q^3 + 475q^2 + 754q + 360) + \gamma_M\gamma_S(60p^3q^3 + 250p^3q^2 + 270p^3q + 80p^3 + 260p^2q^3 + 990p^2q^2 + 1090p^2q + 360p^2 - 5pq^4 + 250pq^3 + 1045pq^2 + 1250pq + 460p + q^5 + 10q^4 + 95q^3 + 350q^2 + 444q + 180)\}.$
5.  $Sz_e(P_H(p, q)) = \frac{1}{2}\rho_{MS}^3(q + 1)^2(p + 1)\{9p^2q + 6p^2 + 12pq + 6p + q^2 + 5q\}.$
6.  $Sz_{ev}(P_H(p, q)) = \frac{1}{120}\rho_{MS}^2\{\gamma_M(180p + 140q + 300p^2 + 120p^3 + 275q^2 + 160q^3 + 25q^4 + 1040pq^2 + 1170p^2q + 400pq^3 + 450p^3q + 10pq^4 + 1350p^2q^2 + 480p^2q^3 + 510p^3q^2 + 180p^3q^3 + 830pq) + \gamma_S(360 + 1080p + 1032q + 960p^2 + 240p^3 + 925q^2 + 285q^3 + 35q^4 + 3q^5 + 2525pq^2 + 2670p^2q + 650pq^3 + 720p^3q - 5pq^4 + 2610p^2q^2 + 720p^2q^3 + 720p^3q^2 + 180p^3q^3 + 2830pq)\}.$
7.  $PI(P_H(p, q)) = \frac{1}{3}\rho_{MS}^2\{27p^2q^2 + 51p^2q + 27p^2 + 48pq^2 + 90pq + 45p + q^3 + 27q^2 + 44q + 18\}.$
8.  $S(P_H(p, q)) = \frac{1}{15}\rho_{MS}^2\{\gamma_M(45 + 180p + 173q + 195p^2 + 60p^3 + 195q^2 + 70q^3 - 3q^5 + 405pq^2 + 435p^2q + 120pq^3 + 120p^3q + 15pq^4 + 270p^2q^2 + 30p^2q^3 + 60p^3q^2 + 480pq) + \gamma_S(315 + 765p + 758q + 570p^2 + 120p^3 + 570q^2 + 130q^3 - 3q^5 + 885pq^2 + 915p^2q + 180pq^3 + 180p^3q + 15pq^4 + 405p^2q^2 + 30p^2q^3 + 60p^3q^2 + 1455pq)\}.$
9.  $Gut(P_H(p, q)) = \frac{1}{15}\rho_{MS}^2\{180p^3q^2 + 360p^3q + 180p^3 + 90p^2q^3 + 810p^2q^2 + 1335p^2q + 630p^2 + 45pq^4 + 360pq^3 + 1275pq^2 + 1620pq + 675p - 9q^5 + 200q^3 + 630q^2 + 664q + 225\}.$
10.  $Mo(P_H(p, q)) = \frac{1}{24}\rho_{MS}^2\{\gamma_M(54 + 84p + 96q + 42p^2 + 48q^2 + 72pq^2 + 72p^2q + 36p^2q^2 + 144pq + 6(-1)^p(q + 1)^2 + 6(-1)^q(p + 1)^2 + 6(-1)^{p+q}(q + 1)^2) + z(72 + 174p + 176q + 102p^2 + 108q^2 + 4q^3 + 84pq^2 + 96p^2q + 36p^2q^2 + 216pq - 6(-1)^p q(q + 1) - 6(-1)^q p(p + 1) + 6(-1)^{p+q} q(q + 1))\}.$
11.  $Mo_e(P_H(p, q)) = \frac{1}{8}\rho_{MS}^2\{84p + 88q + 144pq + 72pq^2 + 72p^2q + 46p^2 + 48q^2 + 36p^2q^2 + 42 + 2(-1)^p(q + 1)^2 + 2(-1)^q(p + 1)^2 + 2(-1)^{p+q}(q + 1)^2\}.$
12.  $Mo_t(P_H(p, q)) = \frac{1}{24}\rho_{MS}^2\{\rho_{MS}(126 + 252p + 264q + 138p^2 + 144q^2 + 216pq^2 + 216p^2q + 108p^2q^2 + 432pq + 6(-1)^p(q + 1)^2 + 6(-1)^q(p + 1)^2 + 6(-1)^{p+q}(q + 1)^2) + \gamma_M(54 + 84p + 96q + 42p^2 + 48q^2 + 72pq^2 + 72p^2q + 36p^2q^2 + 144pq + 6(-1)^p(q + 1)^2 + 6(-1)^q(p + 1)^2 + 6(-1)^{p+q}(q + 1)^2) + \gamma_S(72 + 174p + 176q + 102p^2 + 108q^2 + 4q^3 + 84pq^2 + 96p^2q + 36p^2q^2 + 216pq - 6(-1)^p q(q + 1) - 6(-1)^q p(p + 1) + 6(-1)^{p+q} q(q + 1))\}.$
13.  $w^+ Mo(P_H(p, q)) = \frac{1}{120}\rho_{MS}^2\{\gamma_M(990 + 1440p + 1808q + 570p^2 - 180p^3 + 960q^2 + 40q^3 + 120q^4 + 72q^5 + 2160pq^2 + 2400p^2q - 240pq^3 - 240pq^4 + 3060p^2q^2 + 720p^2q^3 + 360p^3q^2 + 3120pq + 30(-1)^p(6q + 5)(q + 1)^2 + 30(-1)^q(6p + 5)(p + 1)^2 + 30(-1)^{p+q}(6q + 5)(q + 1)^2) + \gamma_S(1440 + 3510p + 3568q + 2490p^2 + 180p^3 + 2700q^2 + 620q^3 + 240q^4 + 72q^5 + 2820pq^2 + 3720p^2q - 480pq^3 - 240pq^4 + 4140p^2q^2 + 720p^2q^3 + 360p^3q^2 + 4800pq - 30(-1)^p q(6q + 5)(q + 1) - 30(-1)^q p(6p + 5)(p + 1) + 30(-1)^{p+q} q(6q + 5)(q + 1))\}.$

14.  $w^+ Mo_e(P_H(p, q)) = \frac{1}{120} \rho_{MS}^3 \{ 4800p + 5224q + 9360pq + 6480pq^2 + 7200p^2q - 720pq^3 - 720pq^4 + 2730p^2 - 180p^3 + 3120q^2 + 200q^3 + 360q^4 + 216q^5 + 9180p^2q^2 + 2160p^2q^3 + 1080p^3q^2 + 2430 + 30(-1)^p(6q + 5)(q + 1)^2 + 30(-1)^q(6p + 5)(p + 1)^2 + 30(-1)^{p+q}(6q + 5)(q + 1)^2 \}.$
15.  $w^+ Mo_t(P_H(p, q)) = \frac{1}{120} \rho_{MS}^2 \{ \gamma_M(990 + 1440p + 1808q + 570p^2 - 180p^3 + 960q^2 + 40q^3 + 120q^4 + 72q^5 + 2160pq^2 + 2400p^2q - 240pq^3 - 240pq^4 + 720p^2q^3 + 360p^3q^2 + 3060p^2q^2 + 3120pq + 30(-1)^p(6q + 5)(q + 1)^2 + 30(-1)^q(6p + 5)(p + 1)^2 + 30(-1)^{p+q}(6q + 5)(q + 1)^2) + \rho_{MS}(2430 + 4800p + 5224q + 2730p^2 - 180p^3 + 3120q^2 + 200q^3 + 360q^4 + 216q^5 + 6480pq^2 + 7200p^2q - 720pq^3 - 720pq^4 + 9180p^2q^2 + 2160p^2q^3 + 1080p^3q^2 + 9360pq + 30(-1)^p(6q + 5)(q + 1)^2 + 30(-1)^q(6p + 5)(p + 1)^2 + 30(-1)^{p+q}(6q + 5)(q + 1)^2) + \gamma_s(1440 + 3510p + 3568q + 2490p^2 + 180p^3 + 2700q^2 + 620q^3 + 240q^4 + 72q^5 + 2820pq^2 + 3720p^2q - 480pq^3 - 240pq^4 + 4140p^2q^2 + 720p^2q^3 + 360p^3q^2 + 4800pq - 30(-1)^p q(6q + 5)(q + 1) - 30(-1)^q p(6p + 5)(p + 1) + 30(-1)^{p+q} q(6q + 5)(q + 1)) \}.$
16.  $w^* Mo(P_H(p, q)) = \frac{1}{40} \rho_{MS}^3 \{ \gamma_M(180 + 270p + 404q + 120p^2 - 90p^3 + 300q^2 + 60q^4 + 36q^5 + 40q^3 + 780pq^2 + 960p^2q - 120pq^3 - 120pq^4 + 1440p^2q^2 + 360p^2q^3 + 180p^3q^2 + 840pq + 30(-1)^p(3q + 2)(q + 1)^2 + 30(-1)^q(3p + 2)(p + 1)^2 + 30(-1)^{p+q}(3q + 2)(q + 1)^2) + \gamma_s(360 + 900p + 1024q + 870p^2 + 90p^3 + 1020q^2 + 320q^3 + 120q^4 + 36q^5 + 1080pq^2 + 1560p^2q - 240pq^3 - 120pq^4 + 1980p^2q^2 + 360p^2q^3 + 180p^3q^2 + 1320pq - 30(-1)^p q(q + 1)(3q + 2) - 30(-1)^q p(p + 1)(3p + 2) + 30(-1)^{p+q} q(q + 1)(3q + 2)) \}.$
17.  $w^* Mo_e(P_H(p, q)) = \frac{1}{40} \rho_{MS}^4 \{ 1110p + 1372q + 2520pq + 2340pq^2 + 2880p^2q - 360pq^3 - 360pq^4 + 840p^2 - 90p^3 + 1140q^2 + 200q^3 + 180q^4 + 108q^5 + 4320p^2q^2 + 1080p^2q^3 + 540p^3q^2 + 540 + 30(-1)^p(3q + 2)(q + 1)^2 + 30(-1)^q(3p + 2)(p + 1)^2 + 30(-1)^{p+q}(3q + 2)(q + 1)^2 \}.$
18.  $w^* Mo_t(P_H(p, q)) = \frac{1}{40} \rho_{MS}^3 \{ \rho_{MS}(540 + 1110p + 1372q + 840p^2 - 90p^3 + 1140q^2 + 200q^3 + 180q^4 + 108q^5 - 360pq^3 - 360pq^4 + 4320p^2q^2 + 1080p^2q^3 + 540p^3q^2 + 2520pq + 2340pq^2 + 2880p^2q + 30(-1)^p(3q + 2)(q + 1)^2 + 30(-1)^q(3p + 2)(p + 1)^2 + 30(-1)^{p+q}(3q + 2)(q + 1)^2) + \gamma_M(180 + 270p + 404q + 120p^2 - 90p^3 + 300q^2 + 40q^3 + 60q^4 + 36q^5 + 780pq^2 + 960p^2q - 120pq^3 - 120pq^4 + 1440p^2q^2 + 360p^2q^3 + 180p^3q^2 + 840pq + 30(-1)^p(3q + 2)(q + 1)^2 + 30(-1)^q(3p + 2)(p + 1)^2 + 30(-1)^{p+q}(3q + 2)(q + 1)^2) + \gamma_s(360 + 900p + 1024q + 870p^2 + 90p^3 + 1020q^2 + 320q^3 + 120q^4 + 36q^5 + 1080pq^2 + 1560p^2q - 240pq^3 - 120pq^4 + 1980p^2q^2 + 360p^2q^3 + 180p^3q^2 + 1320pq - 30(-1)^p q(q + 1)(3q + 2) - 30(-1)^q p(p + 1)(3p + 2) + 30(-1)^{p+q} q(q + 1)(3q + 2)) \}.$

*Proof.* The monolayer  $P_H(p, q)$  contains  $3(p + q) + 2(pq + 2)$  number of vertices and  $3(p + 1)(q + 1)$  number of edges with  $|V_\gamma(P_H(p, q))| = \gamma_M(1 + p + q + pq) + \gamma_s(3 + 2p + 2q + pq)$  and  $|E_\rho(P_H(p, q))| = 3\rho_{MS}(p + 1)(q + 1)$ . The strength-weighted parameters of the various quotient graphs corresponding to the  $\Theta$ -classes of  $P_H(p, q)$  are tabulated in Table 3. Obviously,  $X_{2i}^{H_p}(w) = |V_\gamma(P_H(p, q))| - X_{1i}^{H_p}(w)$  and  $X_{2i}^{H_p}(s) = |E_\rho(P_H(p, q))| - X_{1i}^{H_p}(s) - X_{3i}^{H_p}(s)$ .

Table 3: Strength-weighted parameters of the quotient graphs  $P_H(p, q)/X_{ki}^{H_p}$ ,  $X \in \{H, O, A, P\}$

| $\Theta$ -class                  | Vertex parameters ( $w_v, s_v$ )  | Edge parameters ( $w_e^*/w_e^+, s_e$ )   |
|----------------------------------|---|--|
| $H_i^{H_p}: 1 \leq i \leq q$     | $H_{1i}^{H_p}(w) = i\gamma_s(2+p) + i\gamma_m(1+p)$                     | $H_{3i}^{H_p}(s) = \rho_{MS}(p+1)$       |
|                                  |   | $H_{3i}^{H_p}(w^+) = \rho_{MS}(6p+5)$    |
|                                  | $H_{1i}^{H_p}(s) = \rho_{MS}(3i-1)(p+1)$                                | $H_{3i}^{H_p}(w^*) = \rho_{MS}^2(9p+6)$  |
| $O_i^{H_p}: 1 \leq i \leq p$     | $O_{1i}^{H_p}(w) = \gamma_s(2i+q+iq+1) + i\gamma_m(q+1)$                | $O_{3i}^{H_p}(s) = \rho_{MS}(q+1)$       |
|                                  |   | $O_{3i}^{H_p}(w^+) = \rho_{MS}(6q+5)$    |
|                                  | $O_{1i}^{H_p}(s) = 3i\rho_{MS}(q+1)$                                    | $O_{3i}^{H_p}(w^*) = \rho_{MS}^2(9q+6)$  |
| $A_i^{H_p}: 1 \leq i \leq q$     | $A_{1i}^{H_p}(w) = i(\gamma_m(1+i) + \gamma_s(3+i))/2$                  | $A_{3i}^{H_p}(s) = i\rho_{MS}$           |
|                                  |   | $A_{3i}^{H_p}(w^+) = 6i\rho_{MS}$        |
|                                  | $A_{1i}^{H_p}(s) = i\rho_{MS}(3i+1)/2$                                  | $A_{3i}^{H_p}(w^*) = 9i\rho_{MS}^2$      |
| $A_i^{H_p}: q+1 \leq i \leq p$   | $A_{1i}^{H_p}(w) = (\gamma_m(2i-q-q^2+2iq) + \gamma_s(4i-q-q^2+2iq))/2$ | $A_{3i}^{H_p}(s) = \rho_{MS}(q+1)$       |
|                                  |   | $A_{3i}^{H_p}(w^+) = \rho_{MS}(6q+5)$    |
|                                  | $A_{1i}^{H_p}(s) = \rho_{MS}(q+1)(6i-3q-2)/2$                           | $A_{3i}^{H_p}(w^*) = \rho_{MS}^2(9q+6)$  |
| $A_{-i}^{H_p}: 1 \leq i \leq q$  | $A_{-1i}^{H_p}(w) = (i+1)(i\gamma_m + (i+2)\gamma_s)/2$                 | $A_{-3i}^{H_p}(s) = \rho_{MS}(i+1)$      |
|                                  |   | $A_{-3i}^{H_p}(w^+) = \rho_{MS}(6i+4)$   |
|                                  | $A_{-1i}^{H_p}(s) = 3i\rho_{MS}(i+1)/2$                                 | $A_{-3i}^{H_p}(w^*) = \rho_{MS}^2(9i+3)$ |
| $P_i^{H_p}: 1 \leq i \leq p+q+3$ | $P_{1i}^{H_p}(w) = \gamma_s$  | $P_{3i}^{H_p}(s) = \rho_{MS}$            |
|                                  |   | $P_{3i}^{H_p}(w^+) = 4\rho_{MS}$         |
|                                  | $P_{1i}^{H_p}(s) = 0$   | $P_{3i}^{H_p}(w^*) = 3\rho_{MS}^2$       |

We therefore derive the indices  $TI \in \{W, W_e, W_{ev}, Sz_v, Sz_e, Sz_{ev}, PI, S, Gut, Mo, Mo_e, Mo_t, w^+Mo, w^+Mo_e, w^+Mo_t, w^*Mo, w^*Mo_e, w^*Mo_t\}$  through the expression

$$\begin{aligned}
TI(P_H(p, q)) &= \sum_{i=1}^q TI(P_H(p, q)/H_i^{H_p}) + \sum_{i=1}^p TI(P_H(p, q)/O_i^{H_p}) + \sum_{i=1}^q TI(P_H(p, q)/A_i^{H_p}) + \\
&\quad + \sum_{i=q+1}^p TI(P_H(p, q)/A_i^{H_p}) + \sum_{i=1}^q TI(P_H(p, q)/A_{-i}^{H_p}) + \sum_{i=1}^{p+q+3} TI(P_H(p, q)/P_i^{H_p}).
\end{aligned}$$

□

### 3.3 1T MS<sub>2</sub> monolayers

In this phase of MS<sub>2</sub> monolayers, the metal atom  $M$  is co-ordinated to six adjoining  $S$  atoms octahedrally, with the two  $S$  layers being stacked in the A–B packing mode. It is also claimed to exhibit

several interesting properties such as strong adsorption of functional groups [58], extraordinary hydrogen evolution reaction (HER) catalytic activity [64] and so on. We represent the bitrapezium, hexagonal and parallelogram shapes of 1T  $\text{MS}_2$  monolayers as  $BT_T(n, p, q)$ ,  $H_T(k)$  and  $P_T(p, q)$  respectively with various  $\Theta$ -classes  $X_{\pm i}^{T\#}$ ,  $X \in \{H, A, O, P\}$  as in the previous section. We now inspect the characterization of these polytypes [58, 59] shown in Figure 7 as follows.

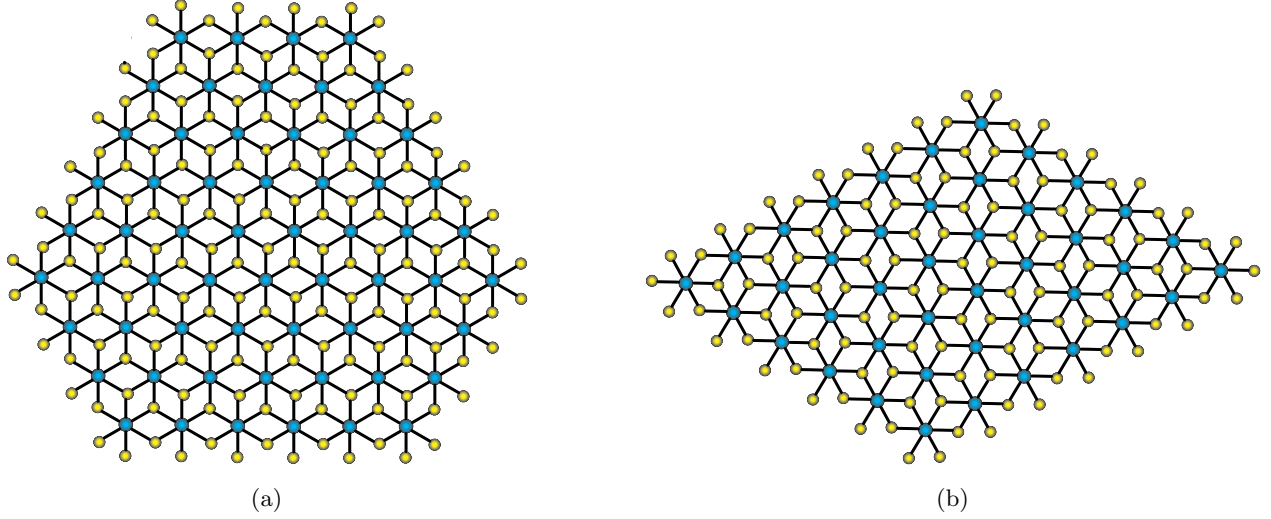


Figure 7: Structure of 1T  $\text{MS}_2$  monolayers (a)  $BT_T(8, 3, 4)$  (b)  $P_T(6, 5)$

**Theorem 7.** For bitrapezium shape 1T  $\text{MS}_2$  monolayer  $BT_T(n, p, q)$ ,  $p + q < n$ , we have

1.  $W(BT_T(n, p, q)) = \frac{1}{60}\{\gamma_M^2(20n^3p^2 + 40n^3pq + 80n^3p + 20n^3q^2 + 80n^3q + 80n^3 - 20n^2p^3 + 30n^2p^2 + 120n^2pq + 230n^2p - 20n^2q^3 - 30n^2q^2 + 110n^2q + 180n^2 + 10np^4 - 20np^3 + 80npq + 150np + 10nq^4 + 20nq^3 + 50nq + 100n - 4p^5 - 10p^4q - 15p^4 - 20p^3q - 30p^3 + 10p^2q + 15p^2 - 10pq^4 - 60pq^3 - 110pq^2 - 40pq + 34p - 4q^5 - 25q^4 - 70q^3 - 95q^2 - 46q) + \gamma_S^2(80n^3p^2 + 160n^3pq + 480n^3p + 80n^3q^2 + 480n^3q + 720n^3 - 80n^2p^3 + 240n^2p^2 + 960n^2pq + 2660n^2p - 80n^2q^3 + 1940n^2q + 3780n^2 + 40np^4 - 160np^3 + 180np^2 + 1760npq + 4480np + 40nq^4 - 60nq^2 + 2760nq + 6060n - 16p^5 - 40p^4q - 80p^4 - 160p^3q - 440p^3 - 140p^2q - 100p^2 - 40pq^4 - 320pq^3 - 860pq^2 + 120pq + 2316p - 16q^5 - 120q^4 - 600q^3 - 1200q^2 + 616q + 3120) + \gamma_M\gamma_S(80n^3p^2 + 160n^3pq + 400n^3p + 80n^3q^2 + 400n^3q + 480n^3 - 80n^2p^3 + 180n^2p^2 + 720n^2pq + 1700n^2p - 80n^2q^3 - 60n^2q^2 + 1100n^2q + 1800n^2 + 40np^4 - 120np^3 + 60np^2 + 920npq + 2060np + 40nq^4 + 40nq^3 - 60nq^2 + 1060nq + 2040n - 16p^5 - 40p^4q - 70p^4 - 120p^3q - 270p^3 - 50p^2q - 110p^2 - 40pq^4 - 280pq^3 - 650pq^2 - 200pq + 646p - 16q^5 - 110q^4 - 430q^3 - 850q^2 - 334q + 540)\}.$
2.  $W_e(BT_T(n, p, q)) = \frac{1}{10}\rho_{MS}^2\{120n^3p^2 + 240n^3pq + 480n^3p + 120n^3q^2 + 480n^3q + 480n^3 - 120n^2p^3 + 360n^2pq + 730n^2p - 120n^2q^3 - 360n^2q^2 + 10n^2q + 490n^2 + 60np^4 + 60np^3 + 180np^2q + 250np^2 + 180npq^2 + 760npq + 820np + 60nq^4 + 300nq^3 + 610nq^2 + 800nq + 570n - 24p^5 - 60p^4q - 135p^4 -$

$$120p^3q - 160p^3 - 90p^2q^2 - 170p^2q - 35p^2 - 60pq^4 - 360pq^3 - 710pq^2 - 430pq + 34p - 24q^5 - 195q^4 - 580q^3 - 765q^2 - 396q - 40\}.$$

3.  $W_{ve}(BT_T(n, p, q)) = \frac{1}{40}\rho_{MS}\{\gamma_M(360n + 86p - 194q + 520n^2 + 320n^3 + 35p^2 - 110p^3 - 75p^4 - 16p^5 - 425q^2 - 330q^3 - 115q^4 - 16q^5 + 80np^2 + 700n^2p - 20np^3 + 320n^3p + 40np^4 + 200nq^2 + 220n^2q + 140nq^3 + 320n^3q + 40nq^4 - 450pq^2 - 30p^2q - 240pq^3 - 80p^3q - 40pq^4 - 40p^4q + 60n^2p^2 - 80n^2p^3 + 80n^3p^2 - 180n^2q^2 - 80n^2q^3 + 80n^3q^2 - 30p^2q^2 + 540np + 340nq - 210pq + 400npq + 60npq^2 + 60np^2q + 360n^2pq + 160n^3pq) + \gamma_s(980 + 3520n + 1062p - 518q + 3000n^2 + 960n^3 - 150p^2 - 490p^3 - 170p^4 - 32p^5 - 1610q^2 - 930q^3 - 250q^4 - 32q^5 + 280np^2 + 2840n^2p - 120np^3 + 800n^3p + 80np^4 + 280nq^2 + 1640n^2q + 200nq^3 + 800n^3q + 80nq^4 - 1290pq^2 - 210p^2q - 560pq^3 - 240p^3q - 80pq^4 - 80p^4q + 240n^2p^2 - 160n^2p^3 + 160n^3p^2 - 240n^2q^2 - 160n^2q^3 + 160n^3q^2 - 60p^2q^2 + 3600np + 2120nq - 500pq + 1880npq + 120npq^2 + 1200n^2pq + 320n^3pq)\}.$
4.  $Sz_v(BT_T(n, p, q)) = \frac{1}{120}\rho_{MS}\{\gamma_M^2(120n^3p^3 + 360n^3p^2q + 720n^3p^2 + 360n^3pq^2 + 1440n^3pq + 1400n^3p + 120n^3q^3 + 720n^3q^2 + 1400n^3q + 880n^3 - 180n^2p^4 - 360n^2p^3q - 540n^2p^3 - 360n^2p^2q^2 - 540n^2p^2q + 420n^2p^2 - 360n^2pq^3 - 900n^2pq^2 + 720n^2pq + 2100n^2p - 180n^2q^4 - 900n^2q^3 - 1020n^2q^2 + 780n^2q + 1320n^2 + 90np^5 + 90np^4q + 180np^3q^2 - 750np^3 + 180np^2q^3 + 360np^2q^2 - 330np^2q - 600np^2 + 90npq^4 - 1050npq^2 - 1320npq + 100np + 90nq^5 + 360nq^4 - 30nq^3 - 1440nq^2 - 1340nq - 40n - 15p^6 + 45p^5 - 45p^4q^2 - 45p^4q + 115p^4 + 90p^3q^2 + 250p^3q + 95p^3 - 45p^2q^4 - 90p^2q^3 + 330p^2q^2 + 855p^2q + 380p^2 + 45pq^4 + 250pq^3 + 585pq^2 + 700pq + 340p - 15q^6 - 45q^5 + 115q^4 + 545q^3 + 620q^2 + 220q) + \gamma_s^2(480n^3p^3 + 1440n^3p^2q + 4000n^3p^2 + 1440n^3pq^2 + 8000n^3pq + 10160n^3p + 480n^3q^3 + 4000n^3q^2 + 10160n^3q + 7920n^3 - 720n^2p^4 - 1440n^2p^3q - 2560n^2p^3 - 1440n^2p^2q^2 - 1440n^2p^2q + 7560n^2p^2 - 1440n^2pq^3 - 2880n^2pq^2 + 16320n^2pq + 33040n^2p - 720n^2q^4 - 4000n^2q^3 - 120n^2q^2 + 24160n^2q + 27720n^2 + 360np^5 + 360np^4q - 520np^4 + 720np^3q^2 - 1440np^3q - 9200np^3 + 720np^2q^3 + 720np^2q^2 - 6000np^2q - 6000np^2 + 360nq^4 - 1440nq^3 - 11760nq^2 - 4640nq + 20520np + 360nq^5 + 920nq^4 - 6960nq^3 - 22800nq^2 - 7640nq + 16680n - 60p^6 + 424p^5 - 180p^4q^2 + 160p^4q + 1680p^4 + 720p^3q^2 + 1280p^3q - 2080p^3 - 180p^2q^4 + 3840p^2q^2 + 5600p^2q - 1020p^2 + 520pq^4 + 1920pq^3 + 1280pq^2 + 2560pq + 6816p - 60q^6 + 64q^5 + 2560q^4 + 5760q^3 + 500q^2 - 2584q + 3840) + \gamma_M\gamma_s(480n^3p^3 + 1440n^3p^2q + 3440n^3p^2 + 1440n^3pq^2 + 6880n^3pq + 7600n^3p + 480n^3q^3 + 3440n^3q^2 + 7600n^3q + 5280n^3 - 720n^2p^4 - 1440n^2p^3q - 2360n^2p^3 - 1440n^2p^2q^2 - 1800n^2p^2q + 4320n^2p^2 - 1440n^2pq^3 - 3240n^2pq^2 + 8880n^2pq + 18200n^2p - 720n^2q^4 - 3800n^2q^3 - 2400n^2q^2 + 11240n^2q + 13200n^2 + 360np^5 + 360np^4q - 260np^4 + 720np^3q^2 - 720np^3q - 5840np^3 + 720np^2q^3 + 1080np^2q^2 - 3600np^2q - 4260np^2 + 360npq^4 - 720npq^3 - 7920npq^2 - 6760npq + 5920np + 360nq^5 + 1180nq^4 - 3280nq^3 - 13620nq^2 - 8640nq + 3600n - 60p^6 + 302p^5 - 180p^4q^2 - 10p^4q + 1030p^4 + 540p^3q^2 + 1160p^3q - 430p^3 - 180p^2q^4 - 180p^2q^3 + 2580p^2q^2 + 4870p^2q + 1070p^2 + 350pq^4 + 1480pq^3 + 2230pq^2 + 2820pq + 2768p - 60q^6 - 58q^5 + 1470q^4 + 4210q^3 + 2910q^2 + 48q + 600)\}.$

5.  $Sz_e(BT_T(n, p, q)) = \frac{1}{2}\rho_{MS}^3\{72n^3p^3 + 216n^3p^2q + 408n^3p^2 + 216n^3pq^2 + 816n^3pq + 772n^3p + 72n^3q^3 + 408n^3q^2 + 772n^3q + 484n^3 - 108n^2p^4 - 216n^2p^3q - 336n^2p^3 - 216n^2p^2q^2 - 432n^2p^2q - 42n^2p^2 - 216n^2pq^3 - 648n^2pq^2 - 168n^2pq + 564n^2p - 108n^2q^4 - 552n^2q^3 - 834n^2q^2 - 144n^2q + 342n^2 + 54np^5 + 54np^4q + 36np^4 + 108np^3q^2 + 120np^3q - 150np^3 + 108np^2q^3 + 336np^2q^2 + 246np^2q + 54npq^4 + 120npq^3 - 66npq^2 - 120npq + 166np + 54nq^5 + 252nq^4 + 306nq^3 - 72nq^2 - 170nq + 66n - 9p^6 + 15p^5 - 27p^4q^2 - 51p^4q + 2p^4 + 18p^3q^2 + 50p^3q + 17p^3 - 27p^2q^4 - 90p^2q^3 - 12p^2q^2 + 195p^2q + 125p^2 + 3pq^4 + 26pq^3 + 117pq^2 + 214pq + 130p - 9q^6 - 39q^5 - 34q^4 + 59q^3 + 107q^2 + 52q + 8\}.$
6.  $Sz_{ev}(BT_T(n, p, q)) = \frac{1}{20}\rho_{MS}^2\{\gamma_M(40 - 20n + 320p + 240q + 940n^2 + 840n^3 + 350p^2 + 85p^3 + 65p^4 + 35p^5 - 15p^6 + 480q^2 + 355q^3 + 35q^4 - 55q^5 - 15q^6 - 330np^2 + 1510n^2p - 510np^3 + 1340n^3p + 30np^4 + 90np^5 - 820nq^2 + 270n^2q + 230nq^3 + 1340n^3q + 390nq^4 + 90nq^5 + 450pq^2 + 650p^2q + 160pq^3 + 180p^3q + 25pq^4 - 65p^4q + 180n^2p^2 - 550n^2p^3 + 700n^3p^2 - 180n^2p^4 + 120n^3p^3 - 1200n^2q^2 - 910n^2q^3 + 700n^3q^2 - 180n^2q^4 + 120n^3q^3 + 175p^2q^2 - 120p^2q^3 + 60p^3q^2 - 45p^2q^4 - 45p^4q^2 + 100np - 890nq + 615pq - 840npq - 360n^2p^2q^2 - 600npq^2 + 20np^2q + 220n^2pq + 100npq^3 + 100np^3q + 1400n^3pq + 90npq^4 + 90np^4q + 460np^2q^2 - 990n^2pq^2 - 630n^2p^2q + 180np^2q^3 + 180np^3q^2 - 360n^2pq^3 - 360n^2p^3q + 360n^3pq^2 + 360n^3p^2q) + \gamma_s(610 + 1120n + 1459p + 859q + 5380n^2 + 2520n^3 + 935p^2 - 60p^3 + 435p^4 + 131p^5 - 30p^6 + 1855q^2 + 1920q^3 + 595q^4 - 49q^5 - 30q^6 - 1660np^2 + 7400n^2p - 2420np^3 + 3640n^3p - 70np^4 + 180np^5 - 5560nq^2 + 4160n^2q - 1100nq^3 + 3640n^3q + 650nq^4 + 180nq^5 + 1190pq^2 + 2350p^2q + 620pq^3 + 500p^3q + 135pq^4 - 45p^4q + 1620n^2p^2 - 1200n^2p^3 + 1680n^3p^2 - 360n^2p^4 + 240n^3p^3 - 1620n^2q^2 - 1920n^2q^3 + 1680n^3q^2 - 360n^2q^4 + 240n^3q^3 + 1060p^2q^2 - 150p^2q^3 + 210p^3q^2 - 90p^2q^4 - 90p^4q^2 + 1970np - 3970nq + 1700pq - 2920npq - 720n^2p^2q^2 - 3080npq^2 - 1120np^2q + 3240n^2pq - 160npq^3 - 160np^3q + 3360n^3pq + 180npq^4 + 180np^4q + 740np^2q^2 - 1800n^2pq^2 - 1080n^2p^2q + 360np^2q^3 + 360np^3q^2 - 720n^2pq^3 - 720n^2p^3q + 720n^3pq^2 + 720n^3p^2q)\}.$
7.  $PI(BT_T(n, p, q)) = \rho_{MS}^2\{36n^2p^2 + 72n^2pq + 140n^2p + 36n^2q^2 + 140n^2q + 140n^2 - 36np^3 - 36np^2q - 40np^2 - 36npq^2 - 16npq + 104np - 36nq^3 - 112nq^2 - 32nq + 106n + 9p^4 - 14p^3 + 18p^2q^2 + 26p^2q - 7p^2 - 10pq^2 - 2pq + 40p + 9q^4 + 22q^3 - 3q^2 - 4q + 42\}.$
8.  $S(BT_T(n, p, q)) = \frac{1}{5}\rho_{MS}\{\gamma_M(30 + 300n + 73p - 127q + 380n^2 + 160n^3 - 5p^2 - 70p^3 - 30p^4 - 8p^5 - 235q^2 - 150q^3 - 50q^4 - 8q^5 + 10np^2 + 470n^2p - 40np^3 + 160n^3p + 20np^4 + 10nq^2 + 230n^2q + 40nq^3 + 160n^3q + 20nq^4 - 240pq^2 - 120pq^3 - 40p^3q - 20pq^4 - 20p^4q + 60n^2p^2 - 40n^2p^3 + 40n^3p^2 - 60n^2q^2 - 40n^2q^3 + 40n^3q^2 + 390np + 170nq - 120pq + 200npq + 240n^2pq + 80n^3pq) + \gamma_s(700 + 2360n + 696p - 364q + 1860n^2 + 480n^3 - 180p^2 - 290p^3 - 70p^4 - 16p^5 - 940q^2 - 450q^3 - 110q^4 - 16q^5 + 80np^2 + 1720n^2p - 120np^3 + 400n^3p + 40np^4 - 40nq^2 + 1120n^2q + 40nq^3 + 400n^3q + 40nq^4 - 690pq^2 - 90p^2q - 280pq^3 - 120p^3q - 40pq^4 - 40p^4q + 180n^2p^2 - 80n^2p^3 + 80n^3p^2 - 60n^2q^2 - 80n^2q^3 + 80n^3q^2 + 2280np + 1240nq - 280pq + 1000npq + 720n^2pq + 160n^3pq)\}.$

$$9. \text{ Gut}(BT_T(n, p, q)) = \frac{2}{5} \rho_{MS}^2 \{ 120n^3p^2 + 240n^3pq + 480n^3p + 120n^3q^2 + 480n^3q + 480n^3 - 120n^2p^3 + 180n^2p^2 + 720n^2pq + 1440n^2p - 120n^2q^3 - 180n^2q^2 + 720n^2q + 1200n^2 + 60np^4 - 120np^3 + 60np^2 + 720npq + 1440np + 60nq^4 + 120nq^3 + 60nq^2 + 720nq + 1195n - 24p^5 - 60p^4q - 90p^4 - 120p^3q - 240p^3 - 60p^2q - 120p^2 - 60pq^4 - 360pq^3 - 780pq^2 - 480pq + 224p - 24q^5 - 150q^4 - 480q^3 - 840q^2 - 496q + 155 \}.$$

Table 4: Strength-weighted parameters of  $BT_T(n, p, q)/X_i^{Tb}$ ,  $X \in \{H, O, A, P\}$

| $\Theta$ -class                          | Edge-strength $X_{3i}^{Tb}(s)$ | Vertex weight $X_{1i}^{Tb}(w)$  | Vertex strength $X_{1i}^{Tb}(s)$                 |
|--|--------------------------------|---|--|
| $H_i^{Tb}: 1 \leq i \leq q+1$            | $\rho_{MS}(2i + 2n - 2q - 1)$  | $(\gamma_s(2i + 2n - 2q + 2i^2 + 4ni - 4iq) + \gamma_M(i^2 - i + 2ni - 2iq))/2$           | $\rho_{MS}(q - n - 4i + 6ni - 6iq + 3i^2 + 1)$   |
| $H_{-i}^{Tb}: 1 \leq i \leq p$           | $\rho_{MS}(2i + 2n - 2p + 1)$  | $(\gamma_s(2 + 6i + 2n - 2p + 2i^2 + 4ni - 4ip) + \gamma_M(i + i^2 + 2ni - 2ip))/2$       | $\rho_{MS}(2i - n + p + 6ni - 6ip + 3i^2)$       |
| $A_i^{Tb}: 1 \leq i \leq p$              | $\rho_{MS}(2i + 2q + 3)$       | $(\gamma_s(4 + 10i + 2q + 2i^2 + 4iq) + \gamma_M(3i + i^2 + 2iq))/2$                      | $\rho_{MS}(8i - q + 6iq + 3i^2 - 1)$             |
| $A_i^{Tb}: p+1 \leq i \leq n-q-1$        | $2\rho_{MS}(p + q + 2)$        | $(\gamma_s(4 + 12i - 2p + 2q - 2p^2 + 4ip + 4iq) + \gamma_M(4i - p - p^2 + 2ip + 2iq))/2$ | $\rho_{MS}(12i - 4p - q + 6ip + 6iq - 3p^2 - 2)$ |
| $A_{-i}^{Tb}: 1 \leq i \leq q+1$         | $\rho_{MS}(2i + 2p + 1)$       | $\gamma_s(p + 1 + i(i + 2p + 3)) + i\gamma_M(i + 2p + 1)/2$                               | $\rho_{MS}(2i - p + 6ip + 3i^2)$                 |
| $P_i^{Tb}: 1 \leq i \leq 2n + p + q + 7$ | $\rho_{MS}$                    | $\gamma_s$  | 0  |

*Proof.* The cardinality of the structural vertex and edge sets of  $BT_T(n, p, q)$  are given as  $|V_\gamma(BT_T(n, p, q))| = (\gamma_M(2 + 4n + p - q - p^2 - q^2 + 2np + 2nq) + \gamma_s(14 + 12n + 4p - 2p^2 - 2q^2 + 4np + 4nq))/2$  and  $|E_\rho(BT_T(n, p, q))| = 3\rho_{MS}(4n + p - q + 2np + 2nq - p^2 - q^2 + 2)$  and which contains  $(16n + 5p - q + 6np + 6nq - 3p^2 - 3q^2 + 16)/2$  vertices and  $3(4n + p - q + 2np + 2nq - p^2 - q^2 + 2)$  edges in the underlying graph.

The strength-weighted parameters of the quotient graphs for various  $\Theta$ -partitions are listed in Table 4 with  $X_{2i}^{Tb}(w) = |V_\gamma(BT_T(n, p, q))| - X_{1i}^{Tb}(w)$  and  $X_{2i}^{Tb}(s) = |E_\rho(BT_T(n, p, q))| - X_{1i}^{Tb}(s) - X_{3i}^{Tb}(s)$ . Thus we now compute the various indices  $TI \in \{W, W_e, W_{ve}, Sz_v, Sz_e, Sz_{ev}, PI, S, Gut\}$  using the expression,

$$TI(BT_T(n, p, q)) = \sum_{i=1}^{q+1} TI(BT_T(n, p, q)/H_i^{Tb}) + \sum_{i=1}^p TI(BT_T(n, p, q)/H_{-i}^{Tb})$$

$$\begin{aligned}
& + 2 \sum_{i=1}^p TI(BT_T(n, p, q) / A_i^{Tb}) + 2 \sum_{i=p+1}^{n-q-1} TI(BT_T(n, p, q) / A_i^{Tb}) \\
& + 2 \sum_{i=1}^{q+1} TI(BT_T(n, p, q) / A_{-i}^{Tb}) + \sum_{i=1}^{2n+p+q+7} TI(BT_T(n, p, q) / P_i^{Tb}).
\end{aligned}$$

□

**Theorem 8.** For  $p + q = n$ , let  $BT_T(n, p, q) = BT_T(n, p)$  be a 1T MS<sub>2</sub> monolayer. Then

1.  $W(BT_T(n, p)) = \frac{1}{60}\{\gamma_M^2(6n^5 + 30n^4p + 45n^4 + 160n^3p + 120n^3 - 60n^2p^3 - 30n^2p^2 + 300n^2p + 135n^2 + 30np^4 - 140np^3 - 60np^2 + 250np + 54n + 40p^4 - 80p^3 - 40p^2 + 80p) + \gamma_S^2(24n^5 + 120n^4p + 360n^4 + 1120n^3p + 2000n^3 - 240n^2p^3 - 480n^2p^2 + 3540n^2p + 5340n^2 + 120np^4 - 800np^3 - 1860np^2 + 4240np + 6676n + 280p^4 - 560p^3 - 1420p^2 + 1700p + 3120) + \gamma_M\gamma_S(24n^5 + 120n^4p + 270n^4 + 880n^3p + 1090n^3 - 240n^2p^3 - 300n^2p^2 + 2280n^2p + 2010n^2 + 120np^4 - 680np^3 - 960np^2 + 2500np + 1706n + 220p^4 - 440p^3 - 760p^2 + 980p + 540)\}.$
2.  $W_e(BT_T(n, p)) = \frac{1}{10}\rho_{MS}^2\{36n^5 + 180n^4p + 225n^4 + 780n^3p + 520n^3 - 360n^2p^3 - 180n^2p^2 + 1290n^2p + 525n^2 + 180np^4 - 480np^3 - 390np^2 + 1120np + 174n + 60p^4 - 120p^3 - 370p^2 + 430p - 20\}.$
3.  $W_{ve}(BT_T(n, p)) = \frac{1}{40}\rho_{MS}\{\gamma_M(166n + 280p + 435n^2 + 410n^3 + 165n^4 + 24n^5 - 180p^2 - 200p^3 + 100p^4 - 240np^2 + 1020n^2p - 440np^3 + 580n^3p + 120np^4 + 120n^4p - 120n^2p^2 - 240n^2p^3 + 840np) + \gamma_S(980 + 3002n + 1580p + 3510n^2 + 1950n^3 + 510n^4 + 48n^5 - 1260p^2 - 640p^3 + 320p^4 - 1740np^2 + 4020n^2p - 1120np^3 + 1640n^3p + 240np^4 + 240n^4p - 600n^2p^2 - 480n^2p^3 + 4200np)\}.$
4.  $Sz_v(BT_T(n, p)) = \frac{1}{120}\rho_{MS}\{\gamma_M^2(15n^6 + 90n^5p + 135n^5 + 90n^4p^2 + 630n^4p + 465n^4 - 240n^3p^3 + 360n^3p^2 + 1590n^3p + 765n^3 - 180n^2p^4 - 1080n^2p^3 + 630n^2p^2 + 1830n^2p + 600n^2 + 360np^5 - 180np^4 - 1560np^3 + 600np^2 + 900np + 180n - 120p^6 + 360p^5 + 60p^4 - 720p^3 + 300p^2 + 120p) + \gamma_S^2(60n^6 + 360n^5p + 984n^5 + 360n^4p^2 + 4200n^4p + 5640n^4 - 960n^3p^3 + 1440n^3p^2 + 17360n^3p + 15040n^3 - 720n^2p^4 - 7680n^2p^3 + 1200n^2p^2 + 33840n^2p + 20580n^2 + 1440np^5 + 960np^4 - 18880np^3 - 3840np^2 + 29720np + 14096n - 480p^6 + 1440p^5 + 4880p^4 - 12160p^3 - 3080p^2 + 9400p + 3840) + \gamma_M\gamma_S(60n^6 + 360n^5p + 762n^5 + 360n^4p^2 + 3360n^4p + 3390n^4 - 960n^3p^3 + 1440n^3p^2 + 11200n^3p + 7110n^3 - 720n^2p^4 - 6000n^2p^3 + 2400n^2p^2 + 17040n^2p + 7470n^2 + 1440np^5 + 120np^4 - 12320np^3 + 1920np^2 + 11560np + 3648n - 480p^6 + 1440p^5 + 2440p^4 - 7280p^3 + 1160p^2 + 2720p + 600)\}.$
5.  $Sz_e(BT_T(n, p)) = \frac{1}{2}\rho_{MS}^3\{9n^6 + 54n^5p + 69n^5 + 54n^4p^2 + 318n^4p + 210n^4 - 144n^3p^3 + 204n^3p^2 + 678n^3p + 327n^3 - 108n^2p^4 - 504n^2p^3 + 294n^2p^2 + 672n^2p + 267n^2 + 216np^5 - 180np^4 - 480np^3 + 186np^2 + 312np + 98n - 72p^6 + 216p^5 - 120p^4 - 120p^3 + 42p^2 + 54p + 8\}.$

6.  $Sz_{ev}(BT_T(n, p)) = \frac{1}{20}\rho_{MS}^2\{\gamma_M(20 + 190n + 60p + 520n^2 + 645n^3 + 405n^4 + 125n^5 + 15n^6 + 235p^2 - 470p^3 - 65p^4 + 360p^5 - 120p^6 + 505np^2 + 1425n^2p - 1190np^3 + 1350n^3p - 240np^4 + 580n^4p + 360np^5 + 90n^5p + 575n^2p^2 - 960n^2p^3 + 350n^3p^2 - 180n^2p^4 - 240n^3p^3 + 90n^4p^2 + 625np) + \gamma_S(470 + 1859n + 560p + 3245n^2 + 3040n^3 + 1515n^4 + 361n^5 + 30n^6 + 1130p^2 - 3140p^3 + 970p^4 + 720p^5 - 240p^6 + 1430np^2 + 6870n^2p - 5420np^3 + 4940n^3p - 60np^4 + 1580n^4p + 720np^5 + 180n^5p + 1270n^2p^2 - 2760n^2p^3 + 700n^3p^2 - 360n^2p^4 - 480n^3p^3 + 180n^4p^2 + 3890np)\}.$
7.  $PI(BT_T(n, p)) = \rho_{MS}^2\{9n^4 + 36n^3p + 50n^3 + 132n^2p + 105n^2 - 72np^3 - 24np^2 + 140np + 102n + 36p^4 - 72p^3 - 8p^2 + 44p + 38\}.$
8.  $S(BT_T(n, p)) = \frac{1}{5}\rho_{MS}\{\gamma_M(30 + 173n + 200p + 315n^2 + 250n^3 + 90n^4 + 12n^5 - 120p^2 - 160p^3 + 80p^4 - 150np^2 + 630n^2p - 280np^3 + 320n^3p + 60np^4 + 60n^4p - 60n^2p^2 - 120n^2p^3 + 570np) + \gamma_S(700 + 1996n + 1060p + 2160n^2 + 1110n^3 + 270n^4 + 24n^5 - 840p^2 - 440p^3 + 220p^4 - 1020np^2 + 2340n^2p - 680np^3 + 880n^3p + 120np^4 + 120n^4p - 300n^2p^2 - 240n^2p^3 + 2640np)\}.$
9.  $Gut(BT_T(n, p)) = \frac{6}{5}\rho_{MS}^2\{12n^5 + 60n^4p + 90n^4 + 320n^3p + 260n^3 - 120n^2p^3 - 60n^2p^2 + 660n^2p + 360n^2 + 60np^4 - 280np^3 - 180np^2 + 640np + 233n + 80p^4 - 160p^3 - 160p^2 + 240p + 55\}.$

*Proof.* In this case, we have the same strength-weight parameter values as in Table 4 for all  $\Theta$ -classess except for the  $\Theta$ -class  $A_p^{Tb}$ , where we have  $A_{3p}^{Tb}(s) = \rho_{MS}(i + p + 2q + 2)$ . The parameter set  $\{n, p, q\}$  also reduces to  $\{n, p, n - p\}$ . Thus following the proof lines of Theorem 7 with the given variation in the parameter set, we obtain the results.

$$\begin{aligned} TI(BT_T(n, p)) &= \sum_{i=1}^{q+1} TI(BT_T(n, p)/H_i^{Tb}) + \sum_{i=1}^p TI(BT_T(n, p)/H_{-i}^{Tb}) \\ &\quad + 2 \sum_{i=1}^{p-1} TI(BT_T(n, p)/A_i^{Tb}) + 2TI(BT_T(n, p)/A_p^{Tb}) \\ &\quad + 2 \sum_{i=1}^q TI(BT_T(n, p)/A_{-i}^{Tb}) + \sum_{i=1}^{2n+p+q+7} TI(BT_T(n, p)/P_i^{Tb}). \end{aligned}$$

□

**Theorem 9.** For hexagonal shape 1T MS<sub>2</sub> monolayer  $H_T(k)$ , we have

1.  $Mo(H_T(k)) = k\rho_{MS}\{\gamma_M(27k^3 + 9k) + \gamma_S(54k^3 + 32k^2 + 30k + 10)\}.$
2.  $Mo_e(H_T(k)) = 18k^2\rho_{MS}^2(9k^2 + 2).$
3.  $Mo_t(H_T(k)) = k\rho_{MS}\{\rho_{MS}(162k^3 + 36k) + \gamma_M(27k^3 + 9k) + \gamma_S(54k^3 + 32k^2 + 30k + 10)\}.$
4.  $w^+ Mo(H_T(k)) = \frac{2}{5}k\rho_{MS}^2\{\gamma_M(1692k^4 - 945k^3 + 360k^2 - 45k - 27) + \gamma_S(3384k^4 + 90k^3 - 520k^2 + 300k + 166)\}.$

5.  $w^+ Mo_e(H_T(k)) = \frac{36}{5} k \rho_{MS}^3 \{564k^4 - 315k^3 + 50k^2 + 5k + 1\}.$
6.  $w^+ Mo_t(H_T(k)) = \frac{2}{5} k \rho_{MS}^2 \{\rho_{MS}(10152k^4 - 5670k^3 + 900k^2 + 90k + 18) + \gamma_M(1692k^4 - 945k^3 + 360k^2 - 45k - 27) + \gamma_s(3384k^4 + 90k^3 - 520k^2 + 300k + 166)\}.$
7.  $w^* Mo(H_T(k)) = \frac{12}{5} k \rho_{MS}^3 \{\gamma_M(564k^4 - 405k^3 + 120k^2 - 45k - 9) + \gamma_s(1128k^4 - 150k^3 - 280k^2 + 22)\}.$
8.  $w^* Mo_e(H_T(k)) = \frac{72}{5} k \rho_{MS}^4 \{564k^4 - 405k^3 + 50k^2 - 15k + 1\}.$
9.  $w^* Mo_t(H_T(k)) = \frac{12}{5} k \rho_{MS}^3 \{\rho_{MS}(3384k^4 - 2430k^3 + 300k^2 - 90k + 6) + \gamma_M(564k^4 - 405k^3 + 120k^2 - 45k - 9) + \gamma_s(1128k^4 - 150k^3 - 280k^2 + 22)\}.$

*Proof.* In  $H_T(k)$ , we have  $H_{3i}^{Th}(w^+) = \rho_{MS}(18(i+k)-11)$ ,  $H_{3i}^{Th}(w^*) = 6\rho_{MS}^2(6(i+k)-5)$ ,  $H_{-3i}^{Th}(w^+) = \rho_{MS}(18(i+k)+7)$ ,  $H_{-3i}^{Th}(w^*) = 6\rho_{MS}^2(6(i+k)+1)$ ,  $P_{3i}^{Th}(w^+) = 7\rho_{MS}$  and  $P_{3i}^{Th}(w^*) = 6\rho_{MS}^2$ . Following the proof lines of Thorem 5, we obtain the indices  $TI \in \{Mo, Mo_e, Mot, w^+ Mo, w^+ Mo_e, w^+ Mot, w^* Mo, w^* Mo_e, w^* Mot\}$  through the expression,

$$TI(H_T(k)) = 3 \sum_{i=1}^k TI(H_T(k)/H_i^{Hh}) + 3 \sum_{i=1}^{k-1} TI(H_T(k)/H_{-i}^{Hh}) + \sum_{i=1}^{3(2k+1)} TI(H_T(k)/P_i^{Hh}).$$

□

**Theorem 10.** For parallelogram shape 1T MS<sub>2</sub> monolayer  $P_T(p, q)$ ,  $1 \leq q \leq p$ , we have

1.  $W(P_T(p, q)) = \frac{1}{60} \{y^2(20p^3q^2 + 40p^3q + 20p^3 + 10p^2q^3 + 90p^2q^2 + 140p^2q + 60p^2 + 5pq^4 + 40pq^3 + 125pq^2 + 130pq + 40p - q^5 + 25q^3 + 60q^2 + 36q) + \gamma_s^2(80p^3q^2 + 320p^3q + 320p^3 + 40p^2q^3 + 720p^2q^2 + 2180p^2q + 1920p^2 + 20pq^4 + 320pq^3 + 2120pq^2 + 4640pq + 3280p - 4q^5 + 340q^3 + 1920q^2 + 3264q + 1800) + y\gamma_s(80p^3q^2 + 240p^3q + 160p^3 + 40p^2q^3 + 540p^2q^2 + 1220p^2q + 720p^2 + 20pq^4 + 240pq^3 + 1160pq^2 + 1860pq + 920p - 4q^5 + 180q^3 + 720q^2 + 904q + 360)\}.$
2.  $W_e(P_T(p, q)) = \frac{1}{15} \rho_{MS}^2 \{180p^3q^2 + 360p^3q + 180p^3 + 90p^2q^3 + 540p^2q^2 + 825p^2q + 360p^2 + 45pq^4 + 360pq^3 + 795pq^2 + 720pq + 210p - 9q^5 + 190q^3 + 360q^2 + 194q\}.$
3.  $W_{ve}(P_T(p, q)) = \frac{1}{30} \rho_{MS} \{y(90p + 83q + 150p^2 + 60p^3 + 150q^2 + 70q^3 - 3q^5 + 315pq^2 + 345p^2q + 120pq^3 + 120p^3q + 15pq^4 + 225p^2q^2 + 30p^2q^3 + 60p^3q^2 + 300pq) + \gamma_s(450 + 1170p + 1156q + 960p^2 + 240p^3 + 960q^2 + 260q^3 - 6q^5 + 1530pq^2 + 1590p^2q + 360pq^3 + 360p^3q + 30pq^4 + 720p^2q^2 + 60p^2q^3 + 120p^3q^2 + 2340pq)\}.$
4.  $Sz_v(P_T(p, q)) = \frac{1}{30} \rho_{MS} \{\gamma_M^2(30p^3q^3 + 90p^3q^2 + 80p^3q + 20p^3 + 90p^2q^3 + 270p^2q^2 + 240p^2q + 60p^2 + 70pq^3 + 210pq^2 + 180pq + 40p + 5q^4 + 30q^3 + 55q^2 + 30q) + \gamma_s^2(120p^3q^3 + 640p^3q^2 + 900p^3q + 320p^3 +$

$$680p^2q^3 + 3240p^2q^2 + 4300p^2q + 1680p^2 - 20pq^4 + 860pq^3 + 4120pq^2 + 5500pq + 2260p + 4q^5 + 20q^4 + 380q^3 + 1660q^2 + 2196q + 900) + \gamma_M\gamma_S(120p^3q^3 + 500p^3q^2 + 540p^3q + 160p^3 + 520p^2q^3 + 1980p^2q^2 + 2120p^2q + 660p^2 - 10pq^4 + 500pq^3 + 1970pq^2 + 2140pq + 680p + 2q^5 + 20q^4 + 210q^3 + 640q^2 + 628q + 180)\}.$$

5.  $Sz_e(P_T(p, q)) = 2\rho_{MS}^3\{18p^3q^3 + 48p^3q^2 + 43p^3q + 12p^3 + 42p^2q^3 + 108p^2q^2 + 93p^2q + 24p^2 + 2pq^4 + 37pq^3 + 82pq^2 + 64pq + 14p + 3q^4 + 16q^3 + 23q^2 + 11q\}.$
6.  $Sz_{ev}(P_T(p, q)) = \frac{1}{60}\rho_{MS}^2\{\gamma_M(360p + 280q + 600p^2 + 240p^3 + 565q^2 + 350q^3 + 65q^4 + 2020pq^2 + 2340p^2q + 770pq^3 + 900p^3q + 20pq^4 + 2700p^2q^2 + 960p^2q^3 + 1020p^3q^2 + 360p^3q^3 + 1630pq) + \gamma_S(900 + 3300p + 3128q + 3480p^2 + 960p^3 + 3430q^2 + 1300q^3 + 170q^4 + 12q^5 + 9680pq^2 + 10680p^2q + 2660pq^3 + 3000p^3q - 20pq^4 + 10440p^2q^2 + 2880p^2q^3 + 2880p^3q^2 + 720p^3q^3 + 10000pq)\}.$
7.  $PI(P_T(p, q)) = \frac{2}{3}\rho_{MS}^2\{54p^2q^2 + 102p^2q + 54p^2 + 96pq^2 + 180pq + 93p + 2q^3 + 54q^2 + 94q + 45\}.$
8.  $S(P_T(p, q)) = \frac{2}{15}\rho_{MS}\{\gamma_M(45 + 180p + 173q + 195p^2 + 60p^3 + 195q^2 + 70q^3 - 3q^5 + 405pq^2 + 435p^2q + 120pq^3 + 120p^3q + 15pq^4 + 270p^2q^2 + 30p^2q^3 + 60p^3q^2 + 480pq) + \gamma_S(720 + 1620p + 1606q + 1140p^2 + 240p^3 + 1140q^2 + 260q^3 - 6q^5 + 1800pq^2 + 1860p^2q + 360pq^3 + 360p^3q + 30pq^4 + 810p^2q^2 + 60p^2q^3 + 120p^3q^2 + 3060pq)\}.$
9.  $Gut(P_T(p, q)) = \frac{2}{5}\rho_{MS}^2\{120p^3q^2 + 240p^3q + 120p^3 + 60p^2q^3 + 540p^2q^2 + 900p^2q + 420p^2 + 30pq^4 + 240pq^3 + 870pq^2 + 1140pq + 475p - 6q^5 + 130q^3 + 420q^2 + 466q + 165\}.$
10.  $Mo(P_T(p, q)) = \frac{1}{12}\rho_{MS}\{\gamma_M(54 + 84p + 96q + 42p^2 + 48q^2 + 72pq^2 + 72p^2q + 36p^2q^2 + 144pq + 6(-1)^p(q + 1)^2 + 6(-1)^q(p + 1)^2 + 6(-1)^{p+q}(q + 1)^2) + \gamma_S(216 + 348p + 376q + 180p^2 + 192q^2 + 8q^3 + 168pq^2 + 192p^2q + 72p^2q^2 + 432pq + 12(-1)^p(q + 2)(q + 1) + 12(-1)^q(p + 2)(p + 1) + 12(-1)^{p+q}(q + 2)(q + 1))\}.$
11.  $Mo_e(P_T(p, q)) = \frac{1}{2}\rho_{MS}^2\{80p + 84q + 144pq + 72pq^2 + 72p^2q + 42p^2 + 44q^2 + 36p^2q^2 + 42 + 6(-1)^p(q + 1)^2 + 6(-1)^q(p + 1)^2 + 6(-1)^{p+q}(q + 1)^2\}.$
12.  $Mo_t(P_T(p, q)) = \frac{1}{12}\rho_{MS}\{\rho_{MS}(252 + 480p + 504q + 252p^2 + 264q^2 + 432pq^2 + 432p^2q + 216p^2q^2 + 864pq + 36(-1)^p(q + 1)^2 + 36(-1)^q(p + 1)^2 + 36(-1)^{p+q}(q + 1)^2) + \gamma_M(54 + 84p + 96q + 42p^2 + 48q^2 + 72pq^2 + 72p^2q + 36p^2q^2 + 144pq + 6(-1)^p(q + 1)^2 + 6(-1)^q(p + 1)^2 + 6(-1)^{p+q}(q + 1)^2) + \gamma_S(216 + 348p + 376q + 180p^2 + 192q^2 + 8q^3 + 168pq^2 + 192p^2q + 72p^2q^2 + 432pq + 12(-1)^p(q + 2)(q + 1) + 12(-1)^q(p + 2)(p + 1) + 12(-1)^{p+q}(q + 2)(q + 1))\}.$
13.  $w^+ Mo(P_T(p, q)) = \frac{1}{30}\rho_{MS}^2\{\gamma_M(540 + 930p + 1392q + 600p^2 - 270p^3 + 1200q^2 + 180q^3 + 180q^4 + 108q^5 + 2700pq^2 + 3420p^2q - 360pq^3 - 360pq^4 + 4680p^2q^2 + 1080p^2q^3 + 540p^3q^2 + 2880pq + 30(-1)^p(9q + 8)(q + 1)^2 + 30(-1)^q(9p + 8)(p + 1)^2 + 30(-1)^{p+q}(9q + 8)(q + 1)^2) + \gamma_S(2160 + 4200p + 5464q +$

$$3420p^2 - 540p^3 + 4800q^2 + 1040q^3 + 720q^4 + 216q^5 + 7440pq^2 + 10920p^2q - 1440pq^3 - 720pq^4 + 12600p^2q^2 + 2160p^2q^3 + 1080p^3q^2 + 9000pq + 60(-1)^p(9q+8)(q+1)(q+2) + 60(-1)^q(9p+8)(p+1)(p+2) + 60(-1)^{p+q}(9q+8)(q+1)(q+2))\}.$$

$$14. \quad w^+ Mo_e(P_T(p, q)) = \frac{1}{5}\rho_{MS}^3 \{860p + 1032q + 2880pq + 2700pq^2 + 3420p^2q - 360pq^3 - 360pq^4 + 600p^2 - 270p^3 + 860q^2 + 60q^3 + 180q^4 + 108q^5 + 4680p^2q^2 + 1080p^2q^3 + 540p^3q^2 + 330 + 30(-1)^p(9q+8)(q+1)^2 + 30(-1)^q(9p+8)(p+1)^2 + 30(-1)^{p+q}(9q+8)(q+1)^2\}.$$

$$15. \quad w^+ Mo_t(P_T(p, q)) = \frac{1}{30}\rho_{MS}^2 \{\rho_{MS}(1980 + 5160p + 6192q + 3600p^2 - 1620p^3 + 5160q^2 + 360q^3 + 1080q^4 + 648q^5 + 16200pq^2 + 20520p^2q - 2160pq^3 - 2160pq^4 + 28080p^2q^2 + 6480p^2q^3 + 3240p^3q^2 + 17280pq + 180(-1)^p(9q+8)(q+1)^2 + 180(-1)^q(9p+8)(p+1)^2 + 180(-1)^{p+q}(9q+8)(q+1)^2) + \gamma_M(540 + 930p + 1392q + 600p^2 - 270p^3 + 1200q^2 + 180q^3 + 180q^4 + 108q^5 + 2880pq + 2700pq^2 + 3420p^2q - 360pq^3 - 360pq^4 + 4680p^2q^2 + 1080p^2q^3 + 540p^3q^2 + 30(-1)^p(9q+8)(q+1)^2 + 30(-1)^q(9p+8)(p+1)^2 + 30(-1)^{p+q}(9q+8)(q+1)^2) + \gamma_S(2160 + 4200p + 5464q + 3420p^2 - 540p^3 + 4800q^2 + 1040q^3 + 720q^4 + 216q^5 + 7440pq^2 + 10920p^2q - 1440pq^3 - 720pq^4 + 12600p^2q^2 + 2160p^2q^3 + 1080p^3q^2 + 9000pq + 60(-1)^p(9q+8)(q+1)(q+2) + 60(-1)^q(9p+8)(p+1)(p+2) + 60(-1)^{p+q}(9q+8)(q+1)(q+2))\}.$$

$$16. \quad w^* Mo(P_T(p, q)) = \frac{1}{5}\rho_{MS}^3 \{\gamma_M(30p + 144q + 60p^2 - 90p^3 + 240q^2 + 60q^3 + 60q^4 + 36q^5 + 660pq^2 + 900p^2q - 120pq^3 - 120pq^4 + 1440p^2q^2 + 360p^2q^3 + 180p^3q^2 + 480pq + 30(-1)^p(3q+2)(q+1)^2 + 30(-1)^q(3p+2)(p+1)^2 + 30(-1)^{p+q}(3q+2)(q+1)^2) + \gamma_S(240p + 568q + 540p^2 - 180p^3 + 960q^2 + 320q^3 + 240q^4 + 72q^5 + 1920pq^2 + 3000p^2q - 480pq^3 - 240pq^4 + 3960p^2q^2 + 720p^2q^3 + 360p^3q^2 + 1560pq + 60(-1)^p(3q+2)(q+1)(q+2) + 60(-1)^q(3p+2)(p+1)(p+2) + 60(-1)^{p+q}(3q+2)(q+1)(q+2))\}.$$

$$17. \quad w^* Mo_e(P_T(p, q)) = \frac{6}{5}\rho_{MS}^4 \{20p + 64q + 480pq + 660pq^2 + 900p^2q - 120pq^3 - 120pq^4 + 60p^2 - 90p^3 + 140q^2 + 20q^3 + 60q^4 + 36q^5 + 1440p^2q^2 + 360p^2q^3 + 180p^3q^2 - 30 + 30(-1)^p(3q+2)(q+1)^2 + 30(-1)^q(3p+2)(p+1)^2 + 30(-1)^{p+q}(3q+2)(q+1)^2\}.$$

$$18. \quad w^* Mo_t(P_T(p, q)) = \frac{1}{5}\rho_{MS}^3 \{\rho_{MS}(120p - 180 + 384q + 360p^2 - 540p^3 + 840q^2 + 120q^3 + 360q^4 + 216q^5 + 3960pq^2 + 5400p^2q - 720pq^3 - 720pq^4 + 2160p^2q^3 + 1080p^3q^2 + 8640p^2q^2 + 2880pq + 180(-1)^p(3q+2)(q+1)^2 + 180(-1)^q(3p+2)(p+1)^2 + 180(-1)^{p+q}(3q+2)(q+1)^2) + \gamma_M(30p + 144q + 60p^2 - 90p^3 + 240q^2 + 60q^3 + 60q^4 + 36q^5 + 660pq^2 + 900p^2q - 120pq^3 - 120pq^4 + 1440p^2q^2 + 360p^2q^3 + 180p^3q^2 + 480pq + 30(-1)^p(3q+2)(q+1)^2 + 30(-1)^q(3p+2)(p+1)^2 + 30(-1)^{p+q}(3q+2)(q+1)^2) + \gamma_S(240p + 568q + 540p^2 - 180p^3 + 960q^2 + 320q^3 + 240q^4 + 72q^5 + 1920pq^2 + 3000p^2q - 480pq^3 - 240pq^4 + 3960p^2q^2 + 720p^2q^3 + 360p^3q^2 + 1560pq + 60(-1)^p(3q+2)(q+1)(q+2) + 60(-1)^q(3p+2)(p+1)(p+2) + 60(-1)^{p+q}(3q+2)(q+1)(q+2))\}.$$

*Proof.* We have  $|V_\gamma(P_T(p, q))| = \gamma_M(p+1)(q+1) + \gamma_S(6 + 4p + 4q + 2pq)$  and  $|E_\rho(P_T(p, q))| = 6\rho_{MS}(p+1)(q+1)$  with the total number of vertices and edges as  $5p + 5q + 3pq + 7$  and  $6(p +$

$1)(q+1)$  respectively. The strength-weighted parameters of all the  $\Theta$ -classes are tabulated in Table 5. Furthermore,  $X_{2i}^{Tp}(w) = |V_\delta(BT_T(n, p, q))| - X_{1i}^{Tp}(w)$  and  $X_{2i}^{Tp}(s) = |E_\zeta(BT_T(n, p, q))| - X_{1i}^{Tp}(s) - X_{3i}^{Tp}(s)$ .

Table 5: Strength-weighted parameters of  $P_T(p, q)/X_{ki}^{Tp}$ ,  $X \in \{H, O, A, P\}$

| $\Theta$ -class                        | Vertex parameters ( $w_v, s_v$ )   | Edge parameters ( $w_e^*/w_e^+, s_e$ )     |
|--|--|--|
| $H_i^{Tp}: 1 \leq i \leq q$            | $H_{1i}^{Tp}(w) = \gamma_s(1 + 4i + p + 2ip)$  | $H_{3i}^{Tp}(s) = 2\rho_{MS}(p + 1)$       |
|  | $+i\gamma_M(p + 1)$  | $H_{3i}^{Tp}(w^+) = 2\rho_{MS}(9p + 8)$    |
|  | $H_{1i}^{Tp}(s) = \rho_{MS}(6i - 1)(p + 1)$  | $H_{3i}^{Tp}(w^*) = 12\rho_{MS}^2(3p + 2)$ |
| $O_i^{Tp}: 1 \leq i \leq p$            | $O_{1i}^{Tp}(w) = \gamma_s(1 + 4i + q + 2iq)$  | $O_{3i}^{Tp}(s) = 2\rho_{MS}(q + 1)$       |
|  | $+i\gamma_M(q + 1)$  | $O_{3i}^{Tp}(w^+) = 2\rho_{MS}(9q + 8)$    |
|  | $O_{1i}^{Tp}(s) = \rho_{MS}(6i - 1)(q + 1)$  | $O_{3i}^{Tp}(w^*) = 12\rho_{MS}^2(3q + 2)$ |
| $A_i^{Tp}: 1 \leq i \leq q$            | $A_{1i}^{Tp}(w) = \gamma_s(1 + 3i + i^2)$  | $A_{3i}^{Tp}(s) = \rho_{MS}(2i + 1)$       |
|  | $+i\gamma_M(i + 1)/2$  | $A_{3i}^{Tp}(w^+) = \rho_{MS}(18i + 7)$    |
|  | $A_{1i}^{Tp}(s) = i\rho_{MS}(3i + 2)$  | $A_{3i}^{Tp}(w^*) = 6\rho_{MS}^2(6i + 1)$  |
| $A_i^{Tp}: q + 1 \leq i \leq p$        | $A_{1i}^{Tp}(w) = (\gamma_s(2 + 8i - 2q - 2q^2 + 4iq) + \gamma_M(2i - q - q^2 + 2iq))/2$ | $A_{3i}^{Tp}(s) = 2\rho_{MS}(q + 1)$       |
|  |  | $A_{3i}^{Tp}(w^+) = 2\rho_{MS}(9q + 8)$    |
|  | $A_{1i}^{Tp}(s) = \rho_{MS}(q + 1)(6i - 3q - 1)$   | $A_{3i}^{Tp}(w^*) = 12\rho_{MS}^2(3q + 2)$ |
| $A_{-i}^{Tp}: 1 \leq i \leq q$         | $A_{-1i}^{Tp}(w) = (i + 1)((i + 2)\gamma_s + i\gamma_M)/2$                               | $A_{-3i}^{Tp}(s) = \rho_{MS}(i + 1)$       |
|  |  | $A_{-3i}^{Tp}(w^+) = \rho_{MS}(6i + 4)$    |
|  | $A_{-1i}^{Tp}(s) = 3i\rho_{MS}(i + 1)/2$   | $A_{-3i}^{Tp}(w^*) = \rho_{MS}(9i + 3)$    |
| $P_i^{Tp}: 1 \leq i \leq 2(p + q + 3)$ | $P_{1i}^{Tp}(w) = \gamma_s$  | $P_{3i}^{Tp}(s) = \rho_{MS}$               |
|  |  | $P_{3i}^{Tp}(w^+) = 7\rho_{MS}$            |
|  | $P_{1i}^{Tp}(s) = 0$   | $P_{3i}^{Tp}(w^*) = 6\rho_{MS}^2$          |

We therefore derive the indices  $TI \in \{W, W_e, W_{ve}, Sz_v, Sz_e, Sz_{ev}, PI, S, Gut, Mo, Mo_e, Mo_t, w^+Mo, w^+Mo_e, w^+Mo_t, w^*Mo, w^*Mo_e, w^*Mo_t\}$  using the expression,

$$\begin{aligned}
TI(P_T(p, q)) &= \sum_{i=1}^q TI(P_T(p, q)/H_i^{Tp}) + \sum_{i=1}^p TI(P_T(p, q)/O_i^{Tp}) + 2 \sum_{i=1}^q TI(P_T(p, q)/A_i^{Tp}) + \\
&\quad + \sum_{i=q+1}^p TI(P_T(p, q)/A_i^{Tp}) + \sum_{i=1}^{2(p+q+3)} TI(P_T(p, q)/P_i^{Tp}).
\end{aligned}$$

□

## 4 Concluding Remarks

We have obtained the relativistic topological indices of two novel 2D transition metal disulfide monolayer materials in their two significant structural phase. We have shown that their graphs belong to a family of partial cubes, a class of graphs whose metric structure is well-understood. The Mostar type indices are hard to produce in closed forms for generalized bitrapezium shapes of  $\text{MS}_2$  monolayers due to some setbacks in finding the absolute differences using the MATLAB interface, whereas a script file can be easily generated from our computations to find the Mostar indices of a particular structure. As the present model includes relativistic quantum effects, it is anticipated that the newly developed model will provide greater insights into the molecular structures and 2D networks of these novel materials. This better understanding of the geometries and behaviors of these high performance thermoelectric materials will enable us to expand their applications in the emerging technology, since the study on their opto-electronic properties is a new, exciting and rapidly growing area of research.

## Acknowledgement

S. Klavžar acknowledges the financial support from the Slovenian Research Agency (research core funding No. P1-0297 and projects J1-9109, J1-1693, N1-0095, N1-0108).

## References

- [1] P. Miro, M. Audiffred, T. Heine, An atlas of two-dimensional materials, *Chem. Soc. Rev.* **43** (2014) 6537–6554.
- [2] M. Xu, T. Liang, M. Shi, H. Chen, Graphene-like two-dimensional materials, *Chem. Rev.* **113** (2013) 3766–3798.
- [3] K.F. Mak, C. Lee, J. Hone, J. Shan, T.F. Heinz, Atomically thin  $\text{MoS}_2$ : A new direct-gap semiconductor, *Phys. Rev. Lett.* **105** (2010) 136805.
- [4] Q.H. Wang, K. Kalantar-Zadeh, A. Kis, J.N. Coleman, M.S. Strano, Electronics and optoelectronics of two-dimensional transition metal dichalcogenides, *Nat. Nanotechnol.* **7** (2012) 699–712.
- [5] K.S. Novoselov, D. Jiang, F. Schedin, T.J. Booth, V.V. Khotkevich, S.V. Morozov, A.K. Geim AK, Two-dimensional atomic crystals, *Proc. Natl. Acad. Sci. U.S.A.* **102** (2005) 10451–10453.

- [6] B. Radisavljevic, A. Radenovic, J. Brivio, V. Giacometti, A. Kis, Single-layer MoS<sub>2</sub> transistors, *Nat. Nano.* **6** (2011) 147–150.
- [7] H. Babaei, J.M. Khodadadi, S. Sinha, Large theoretical thermoelectric power factor of suspended single-layer MoS<sub>2</sub>, *Appl. Phys. Lett.* **105** (2014) 193901.
- [8] G. Plechinger, P. Nagler, A. Arora, R. Schmidt, A. Chernikov, A.G.D. Águila, P.C.M. Christiaanen, R. Bratschitsch, C. Scüller, T. Korn, Trion fine structure and coupled spin-valley dynamics in monolayer tungsten disulfide, *Nat. Commun.* **7** (2016) 12715.
- [9] W. Schutte, J.D. Boer, F. Jellinek, Crystal structures of tungsten disulfide and diselenide, *J. Solid State Chem.* **70**(2) (1987) 207–209.
- [10] G.X. Wang, S. Bewlay, J. Yao, H.K. Liu, S.X. Dou, Tungsten disulfide nanotubes for lithium storage, *Electrochem. Solid-State Lett.* **7**(10) (2004) A321–A323.
- [11] B.K. Miremadi, S.R. Morrison, The intercalation and exfoliation of tungsten disulfide, *J. Appl. Phys.* **63**(10) (1988) 4970–4974.
- [12] V. Carozo, Y. Wang, K. Fujisawa, B.R. Carvalho, A. McCreary, S. Feng, Z. Lin, C. Zhou, N. Perea-López, A.L. Elías, B. Kabius, V.H. Crespi, M. Terrones, Optical identification of sulfur vacancies: Bound excitons at the edges of monolayer tungsten disulfide, *Sci. Adv.* **3**(4) (2017) e1602813.
- [13] Z. He, W. Xu, Y. Zhou, X. Wang, Y. Sheng, Y. Rong, S. Guo, J. Zhang, J.M. Smith, J.H. Warner, Biexciton formation in bilayer tungsten disulfide, *ACS Nano* **10**(2) (2016) 2176–2183.
- [14] L. Kou, A. Du, C. Chen, T. Frauenheim, Strain engineering of selective chemical adsorption on monolayer MoS<sub>2</sub>, *Nanoscale* **6** (2014) 5156–5161.
- [15] A. Kuc, N. Zibouche, T. Heine, Influence of quantum confinement on the electronic structure of the transition metal sulfide TS<sub>2</sub>, *Phys. Rev. B* **83** (2011) 245213.
- [16] K.F. Mak, J. Shan, Photonics and optoelectronics of 2D semiconductor transition metal dichalcogenides, *Nat. Photonics* **10** (2016) 216–226.
- [17] Y. Zhang, Y. Zhang, Q. Ji, J. Ju, H. Yuan, J. Shi, T. Gao, D. Ma, M. Liu, Y. Chen, X. Song, H.Y. Hwang, Y. Cui, Z. Liu, Controlled growth of high-quality monolayer WS<sub>2</sub> layers on sapphire and imaging its grain boundary, *ACS Nano* **7**(10) (2013) 8963–8971.

- [18] D. Xiao, G.-B. Liu, W. Feng, X. Xu, W. Yao, Coupled spin and valley physics in monolayers of MoS<sub>2</sub> and other group-VI dichalcogenides, *Phys. Rev. Lett.* **108** (2012) 196802.
- [19] K. Balasubramanian, Relativistic effects in chemistry, Part A: Theory and techniques, Wiley, New York, 1997.
- [20] K. Balasubramanian, D. Dai, Electronic states and potential energy surfaces of the tungsten trimer (W<sub>3</sub>), *Chem. Phys. Lett.* **265**(3-5) (1997) 538–546.
- [21] K. Balasubramanian, Spectroscopic constants and potential energy curves of tungsten carbide, *J. Chem. Phys.* **112**(17) (2000) 7425–7436.
- [22] H. Hwang, H. Kim, J. Cho, MoS<sub>2</sub> nanoplates consisting of disordered graphene-like layers for high rate lithium battery anode materials, *Nano Lett.* **11** (2011) 4826–4830.
- [23] S. Bertolazzi, J. Brivio, A. Kis, Stretching and breaking of ultrathin MoS<sub>2</sub>, *ACS Nano* **5** (2011) 9703–9709.
- [24] G. Eda, H. Yamaguchi, D. Voiry, T. Fujita, M. Chen, M. Chhowalla, Photoluminescence from chemically exfoliated MoS<sub>2</sub>, *Nano Lett.* **11**(12) (2011) 5111–5116.
- [25] K. Mak, K. He, J. Shan, T.F. Heinz, Control of valley polarization in monolayer MoS<sub>2</sub> by optical helicity, *Nat. Nanotechnol.* **7** (2012) 494–498.
- [26] S. Manzeli, D. Ovchinnikov, D. Pasquier, O.V. Yazyev, A. Kis, 2D transition metal dichalcogenides, *Nat. Rev. Mater.* **2** (2017) 17033.
- [27] S.C. Basak, K. Balasubramanian, B.D. Gute, D. Mills, A. Gorczynska, S. Roszak, Prediction of cellular toxicity of halocarbons from computed chemodescriptors: A hierarchical QSAR approach, *J. Chem. Inf. Comput. Sci.* **43**(4) (2003) 1103–1109.
- [28] S.C. Basak, D. Mills, M.M. Mumtaz, Quantitative structure-activity relationship (QSAR) study of dermal absorption using theoretical molecular descriptors, *SAR QSAR Environ. Res.* **18**(1–2) (2007) 45–55.
- [29] H. Wiener, Structural determination of paraffin boiling points, *J. Am. Chem. Soc.* **69**(1) (1947) 17–20.
- [30] M. Randić, Topological indices, in: P. von Rague Schleyer (Ed.), *Encyclopedia of Computational Chemistry*, Wiley, London, 1998, pp. 3018–3032.

- [31] M. Arockiaraj, J. Clement, N. Tratnik, Mostar indices of carbon nanostructures and circumscribed donut benzenoid systems, *Int. J. Quantum Chem.* **119**(24) (2019) e26043.
- [32] M. Arockiaraj, S. Klavžar, J. Clement, S. Mushtaq, K. Balasubramanian, Edge distance-based topological indices of strength-weighted graphs and their application to coronoid systems, carbon nanocones and SiO<sub>2</sub> nanostructures, *Mol. Inform.* **38**(11-12) (2019) 1900039.
- [33] M. Arockiaraj, J. Clement, K. Balasubramanian, Topological indices and their applications to circumcised donut benzenoid systems, kekulenes and drugs, *Polycycl. Aromat. Comp.* **40**(2) (2020) 280–303.
- [34] M. Črepnjak, N. Tratnik, The Szeged index and the Wiener index of partial cubes with applications to chemical graphs, *Appl. Math. Comput.* **309** (2017) 324–333.
- [35] N. Tratnik, The edge-Szeged index and the PI index of benzenoid systems in linear time, *MATCH Commun. Math. Comput. Chem.* **77**(2) (2017) 393–406.
- [36] T. Došlić, I. Martinjak, R. Škrekovski, S.T. Spužević, I. Zubac, Mostar index, *J. Math. Chem.* **56** (2018) 2995–3013.
- [37] R. Carbó-Dorca, T. Chakraborty, Divagations about the periodic table: Boolean hypercube and quantum similarity connections, *J. Comput. Chem.* **40**(30) (2019) 2653–2663.
- [38] J.R. Dias, Handbook of polycyclic hydrocarbons. Part A: Benzenoid hydrocarbons, Elsevier, United States, 1987, pp. 400.
- [39] I. Gutman, N. Trinajstić, Graph theory and molecular orbitals: The loop rule, *Chem. Phys. Lett.* **20**(3) (1973) 257–260.
- [40] J.C. Dobrowolski, The structural formula version of graph theory, *MATCH Commun. Math. Comput. Chem.* **81** (2019) 527–555.
- [41] M. Arockiaraj, S.R.J. Kavitha, S. Mushtaq, K. Balasubramanian, Relativistic topological molecular descriptors of metal trihalides, *J. Mol. Struc.* **1217** (2020) 128368.
- [42] H.P. Schultz, T.P. Schultz, Topological organic chemistry. 7. Graph theory and topological indices of cycloalkanes, *J. Chem. Inf. Comput. Sci.* **33** (1993) 863–867.
- [43] I. Gutman, Selected properties of the Schultz molecular topological index, *J. Chem. Inf. Comput. Sci.* **34** (1994) 1087–1089.

- [44] M. Arockiaraj, S.R.J. Kavitha, K. Balasubramanian, I. Gutman, Hyper-Wiener and Wiener polarity indices of silicate and oxide frameworks, *J. Math. Chem.* **56**(5) (2018) 1493–1510.
- [45] S. Klavžar, M.J. Nadjafi-Arani, Cut method: Update on recent developments and equivalence of independent approaches, *Curr. Org. Chem.* **19**(4) (2015) 348–358.
- [46] D. Djoković, Distance preserving subgraphs of hypercubes, *J. Combin. Theory Ser. B* **14**(3) (1973) 263–267.
- [47] P. Winkler, Isometric embeddings in products of complete graphs, *Discrete Appl. Math.* **7**(2) (1984) 221–225.
- [48] M. Chhowalla, H.S. Shin, G. Eda, L.-J. Li, K.P. Loh, H. Zhang, The chemistry of two-dimensional layered transition metal dichalcogenide nanosheets, *Nat. Chem.* **5** (2013) 263–275.
- [49] C. Ataca, H. Şahin, S. Ciraci, Stable, single-layer MX<sub>2</sub> transition-metal oxides and dichalcogenides in a honeycomb-like structure, *J. Phys. Chem. C* **116**(16) (2012) 8983–8999.
- [50] J. Heising, M.G. Kanatzidis, Structure of restacked MoS<sub>2</sub> and WS<sub>2</sub> elucidated by electron crystallography, *J. Am. Chem. Soc.* **121**(4) (1999) 638–643.
- [51] F. Wypych, R. Schöllhorn, 1T-MoS<sub>2</sub>, a new metallic modification of molybdenum-disulfide, *J. Chem. Soc., Chem. Commun.* **19** (1992) 1386–1388.
- [52] K. Balasubramanian, Cas scf/ci calculations on Si<sub>4</sub> and Si<sub>4</sub><sup>+</sup>, *Chem. Phys. Lett.* **135**(3) (1987) 283–287.
- [53] K. Balasubramanian, Relativistic calculations of electronic states and potential energy surfaces of Sn<sub>3</sub>, *J. Chem. Phys.* **85**(6) (1986) 3401–3406.
- [54] K. Balasubramanian, Ten low-lying electronic states of Pd<sub>3</sub>, *J. Chem. Phys.* **91**(1) (1989) 307–313.
- [55] J. Pipek, P.G. Mezey, A fast intrinsic localization procedure applicable for ab initio and semiempirical linear combination of atomic orbital wave functions, *J. Chem. Phys.* **90**(9) (1989) 4916–4926.
- [56] Y. Kang, S. Najmaei, Z. Liu, Y. Bao, Y. Wang, X. Zhu, N.J. Halas, P. Nordlander, P.M. Ajayan, J. Lou, Z. Fang, Plasmonic hot electron induced structural phase transition in a MoS<sub>2</sub> monolayer, *Adv. Mater.* **26**(37) (2014) 6467–6471.

- [57] M. Kan, J.Y. Wang, X.W. Li, S.H. Zhang, Y.W. Li, Y. Kawazoe, Q. Sun, P. Jena, Structures and phase transition of a MoS<sub>2</sub> monolayer, *J. Phys. Chem. C* **118** (2014) 1515–1522.
- [58] Q. Tang, D.E. Jiang, Stabilization and band-gap tuning of the 1T-MoS<sub>2</sub> monolayer by covalent functionalization, *Chem. Mater.* **27** (2015) 3743–3748.
- [59] H. Huang, Y. Cui, Q. Li, C. Dun, W. Zhou, W. Huang, L. Chen, C.A. Hewitt, D.L. Carroll, Metallic 1T phase MoS<sub>2</sub> nanosheets for high-performance thermoelectric energy harvesting, *Nano Energy* **26** (2016) 172–179.
- [60] S. Klavžar, I. Gutman, B. Mohar, Labeling of benzenoid systems which reflects the vertex distance relations, *J. Chem. Inf. Comput. Sci.* **35**(3) (1995) 590–593.
- [61] V. Chepoi, *d*-Convexity and isometric subgraphs of Hamming graphs, *Cybernetics* **24**(1) (1988) 6–11.
- [62] K.Q. Dang, D.E. Spearot, Effect of point and grain boundary defects on the mechanical behavior of monolayer MoS<sub>2</sub> under tension via atomistic simulations, *J. Appl. Phys.* **116**(1) (2014) 013508.
- [63] W. Zhou, X. Zou, S. Najmaei, Z. Liu, Y. Shi, J. Kong, J. Lou, P.M. Ajayan, B.I. Yakobson, J.-C. Idrobo, Intrinsic structural defects in monolayer molybdenum disulfide, *Nano Lett.* **13**(6) (2013) 2615–2622.
- [64] M.A. Lukowski, A.S. Daniel, F. Meng, A. Forticaux, L. Li, S. Jin, Enhanced hydrogen evolution catalysis from chemically exfoliated metallic MoS<sub>2</sub> nanosheets, *J. Am. Chem. Soc.* **135**(28) (2013) 10274–10277.